COMET-Projekt Rail4Future
Resilient Digital Railway Systems to enhance performance

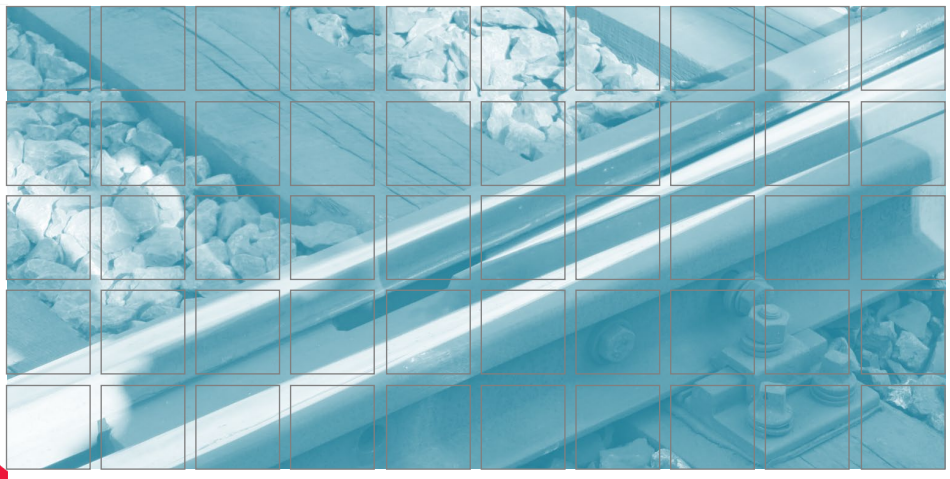

D2.2.3 Report on available historical Data and identified further required Data

D2.2.5 Report on the descriptive Model

2022

Markus Loidolt
Dipl.-Ing.
+43 316 873 4994
markus.loidolt@tugraz.at

Stefan Marschnig
Assoc.Prof. Dipl.-Ing. Dr.tech
+43 664 60 873 6717
stefan.marschnig@tugraz.at

Preface

Although one of the most safety-critical and highly stressed components of the railway track (due to dynamic impact loads and slip), decisions regarding necessary maintenance activities and renewals of turnouts are still made on the basis of visual inspections. This approach builds on the extensive experience of those responsible for the system and ensures safe operation, but also comes with critical disadvantages. The inspection is time-consuming and expensive, and employees are in the danger zone. A particularly critical aspect is that assuming a same number of qualified employees available in the medium term (labour market situation) is simply unrealistic. In addition, it can be assumed that the population will demand a higher utilisation of the railway network (climate change) increasing the loads on the components and at the same time shortening the time slots for inspection and maintenance. For these reasons, one of the aims of the project is to advance the condition assessment of frogs using measurement data and thus to provide the responsible railway staff a tool supporting their decision-making processes.

Content

1 D2.2.3. Report on available historical Data and identified further required Data (M18)

The descriptive approach should provide verified prediction algorithms and trend analysis concepts for turnouts. These algorithms need to be derived on a sound data basis. For this reason, in the first project phase, necessary data for further work were defined and requests were made to the corresponding project partners. In the following, we address this data and show to what extent this data is available.

1.1 Basic data for the algorithm development

A description of the necessary data has already been given in "D2.2.2 Report of Requirements", the data sources described there are:

- Data measured by the track recoding car EM250/EM160
  - Half gauge unfiltered
  - Half gauge filtered
  - Alignment (D1, D2)
  - Longitudinal level (D1, D2)
  - Rail surface signal (RSS)
  - Axle Box Accelerations (ABA)
- Metadata of turnouts
- Documented executed maintenance actions
- Geometry measurements (Calipri) of selected frogs
- Turnouts layouts (technical drawings)

The listed data (with the exception of the Calipri measurements) are available for the 30 project turnouts or can be supplied by ÖBB on request. Calipri measurements are available for the crossing of one turnout. Voestalpine is currently preparing the data source for two other selected frogs to provide it in the near future.

1.2 Additional data for algorithm validation

In addition to the data described, more data is used for the validation of the algorithms. These data sources are not available on a network-wide basis, but for some of the turnouts.

1.2.1 ÖBB – measurements with mobile system

ÖBB is currently running a measurement campaign measuring frog geometry, accelerations occurring at the frog due to train crossings and the wheel-impact-point by a mobile measurement system. Both, the acceleration data and the frog geometry data, can be used for a validation of the developed algorithms. Examples of acceleration data have already been transmitted for selected turnouts (Figure 1)

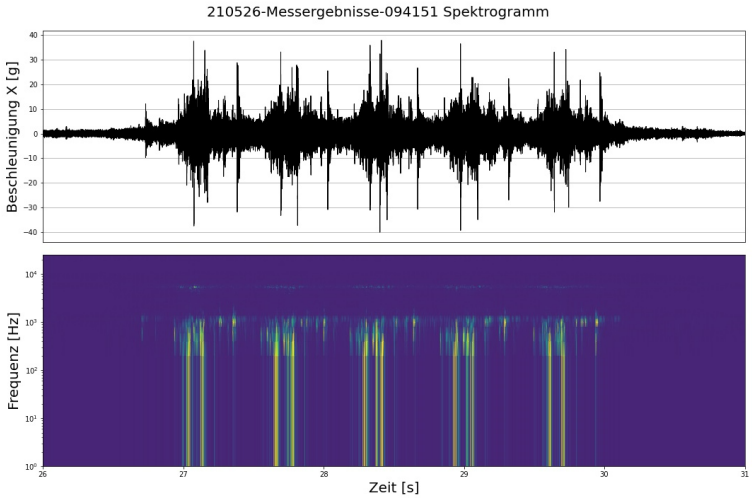

Figure 1 - Acceleration data, received from a mobile system

1.2.2 Wayside train monitoring checkpoints

The quality behaviour of turnout components depends on the component properties, system interactions and the amount of load. The description of the load as gross-tonnes per day is a rough approximation; for differentiated analyses, differentiated information about the type of loading is necessary. Of major importance is the number of axles passing, the load applied per axle and the proportion of unsprung mass. For some questions, the condition of the wheels can also be essential, although, in the descriptive approach this parameter can only be included as an average value for the entire vehicle collective. The information described here is recorded by the wayside train monitoring checkpoints distributed in the network. In the course of the project meetings, this data was requested for the checkpoint in Niklasdorf and ÖBB has already agreed that the data can be used within

the project. As soon as available, the detailed loading information can be considered in the assessment of the project turnouts in Niklasdorf.

1.2.3 Sensor concept - Niklasdorf

A cooperation between Area 2.2 and Area 2.1 (several project partners are involved) aims at equipping one of the project turnouts with a comprehensive sensor concept. The concept (Figure 2) was developed by the project consortium and is expected to be put into operation in 2022.

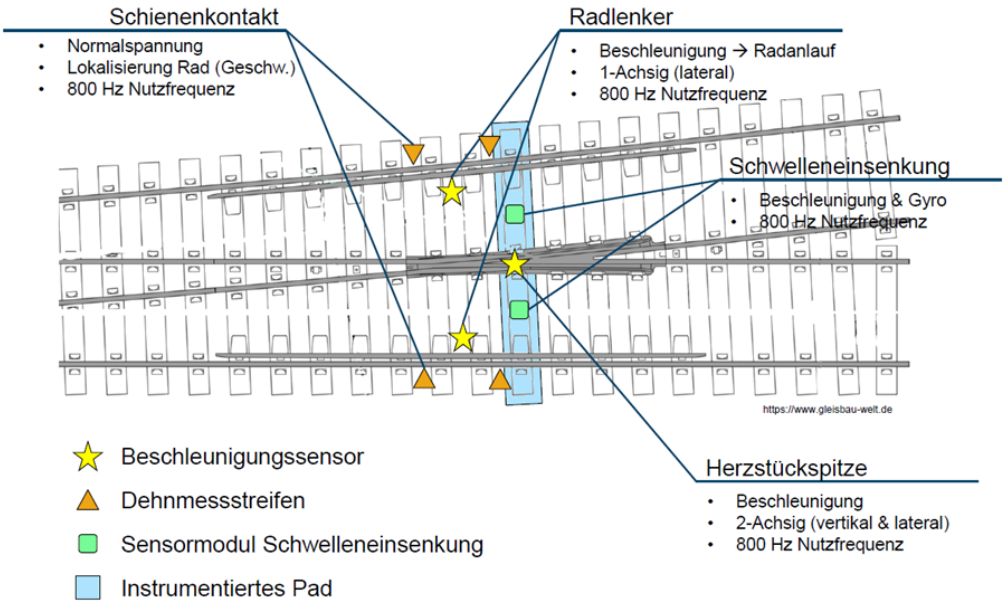

Figure 2 - Sensor concept for one of the project turnouts

Although the sensor concept was created for the simulative approach, the measured data can be used perfectly for validation and, if necessary, for adaptation of the descriptive algorithms. In particular, the data on the sleeper deflection and the acceleration values at the frog will be used for these issues. Additionally, a comparison with the measured variables from the EM 250 is thinkable.

1.2.4 Chord-measurements (track geometry)

As described later on in this report (2.2.3), there are some open questions regarding the measurements of the track geometry by means of an inertial measurement system at the position of the frog. Here, chord measurements can be used as a comparison. In Austria, these measuring systems are mainly installed on tamping machines (for measurements before/after tamping). A data request has already been made.

1.2.5 EM 250 – condition of wheels

Since the axle box acceleration data of the measuring car is used for the condition assessment of frogs (2.2.5), the question of the wheel condition arises, as it has a dominant influence on the frog transition. It is assumed that the wheel condition is kept at a good level, as other measuring systems would also be influenced by wheel irregularities. Nevertheless, a potential influence should be analysed. Detailed information of the standard profile as well as the worst possible condition (directly before the maintenance of the wheels) allow quantifying the potential influence of the wheel condition on the measured axle box accelerations. The data request was made at the last status meeting and is currently being processed.

1.3 Conclusions on historical data available

A list of 30 turnouts (Table 1) was defined for further evaluations. Basic data is available for 29 of these 30 turnouts and could already be used for the implementation of descriptive algorithms. Additional data is and/or will be also available for selected turnouts for validation means. The milestones "Historical data available" and "Further required data identified" can therefore be regarded as completed. Of course, the research project character goes along with the fact that new arising questions might lead to the necessity of additional data.

Table 1 - List of project turnouts

Turnout	Location	Local Number	DB776	Position	Type	Crossing nose material
T_R4F_1	Bf. Niklasdorf	1	8130	10,527	EW-60E1-500-12-Fz-Be-be	CENTRO Mn13 EDH
T_R4F_2	Bf. Niklasdorf	2	8130	10,626	EW-60E1-500-12-Fz-Be-be	CENTRO Mn13 EDH
T_R4F_3	Bf. Niklasdorf	5	8130	10,674	EW-60E1-500-12-Fz-Be-be	CENTRO Mn13 EDH
T_R4F_4	Bf. Niklasdorf	6	8130	10,773	EW-60E1-500-12-Fz-Be-be	CENTRO Mn13 EDH
T_R4F_5	Bf. Niklasdorf	53	8130	11,949	EW-60E1-500-12-Fz-Be-be	W360
T_R4F_6	Bf. Niklasdorf	54	8130	12,048	EW-60E1-500-12-Fz-Be-be	400UHC/K600
T_R4F_7	Bf. Niklasdorf	62	8130	12,119	EW-60E1-500-12-Fz-Be-be	400UHC/K600
T_R4F_8	Bf. Niklasdorf	63	8130	12,218	EW-60E1-500-12-Fz-Be-be	W360
T_R4F_9	Bf. Wels	126	4012	213,31	EW-54E2-500-12-FSch-H	COMPOUND Mn13
T_R4F_10	Bf. Wels	127	4012	213,41	EW-54E2-500-12-FSch-H	COMPOUND Mn13
T_R4F_11	Bf. Wels	128	4012	213,41	EW-54E2-500-12-FSch-H	COMPOUND Mn13
T_R4F_12	Bf. Wels	129	4012	213,505	ABW/IBW-54E2-500-12-FSch-H	COMPOUND Mn13
T_R4F_13	Bf. Wels	130	4012	213,519	EW-54E2-500-12-FSch-H	CENTRO Mn13
T_R4F_14	Bf. Wels	131	4012	213,529	EW-54E2-500-12-FSch-H	CENTRO Mn13 EDH
T_R4F_15	Bf. Zeltweg	59	8131	232,521	EW-60E1-500-12-Fz-Be-be	DB Witten Chrom Bainit
T_R4F_16	Bf. Zeltweg	61	8131	232,531	EW-60E1-500-12-Fz-Be-be	BWG Chrom Bainit
T_R4F_17	Bf. Zeltweg	62	8131	232,629	EW-60E1-500-12-Fz-Be-be	DB Witten Chrom Bainit
T_R4F_18	Bf. Zeltweg	54	8131	232,426	EW-49E1-190-9-FSch-H	keine Messdaten!!
T_R4F_19	Bf. Zeltweg	67	8131	232,9	IBW-60E1-500-12-Fz-Be-be	CENTRO Mn13 EDH
T_R4F_20	Bf. Zeltweg	68	8131	232,997	ABW-60E1-500-12-Fz-Be-be	DB Witten Chrom Bainit
T_R4F_21	Bf. Marein/ St. Lorenzen	51	8051	147,386	EW-60E1-500-12-Fz-Be-be	VC Mn13
T_R4F_22	Bf. Marein/ St. Lorenzen	53	8051	147,415	EW-60E1-500-12-Fz-Be-be	CENTRO Mn13 EDH
T_R4F_23	Bf. Marein/ St. Lorenzen	54	8051	147,512	EW-60E1-500-12-Fz-Be-be	Bainit Prestige
T_R4F_24	Bf. Marein/ St. Lorenzen	55	8051	147,519	EW-60E1-500-12-Fz-Be-be	Bainit Prestige
T_R4F_25	Bf. Marein/ St. Lorenzen	56	8051	147,619	EW-60E1-500-12-Fz-Be-be	CENTRO Mn13 EDH
T_R4F_26	Bf. Atzgersdorf	1	2052	7,72	ABW-60E1-500-12-Fz-Be-be	-
T_R4F_27	Bf. Atzgersdorf	2	2052	7,827	IBW-60E1-500-12-Fz-Be-be	-
T_R4F_28	Bf. Atzgersdorf	3	2052	7,827	IBW-60E1-500-12-Fz-Be-be	-
T_R4F_29	Bf. Atzgersdorf	4	2052	7,938	ABW-60E1-500-12-Fz-Be-be	-
T_R4F_30	Bf. Atzgersdorf	5	2052	7,948	IBW-60E1-500-12-Fz-Be-be	-

2 D2.2.5 Report on the descriptive Model (M18)

The descriptive approach sets itself the task of preparing and intersecting existing data sources in such a way that a condition assessment of turnout components and a prediction of maintenance activities that will be necessary in the future is possible. A prerequisite for this is sufficient data quality; if this is not ensured, conclusions cannot bring any added value. If sufficient data quality is given, but in the wrong form or without the correct localisation, appropriate processing methods can remedy the situation.

2.1 Positioned data as a precondition for further evaluations

Since the development of the algorithms is largely based on data from the measuring car of the open track, considerations must be made with regard to the positioning accuracy. This corresponds to the requirements of the open track (line infrastructure), and is insufficient for the evaluation of turnouts and especially for the evaluation of individual turnout components (point infrastructure). For this reason, we use the positioning methodology from [1] and adapted it to meet the requirements of the project. The core principle of the positioning process can be seen in Figure 3.

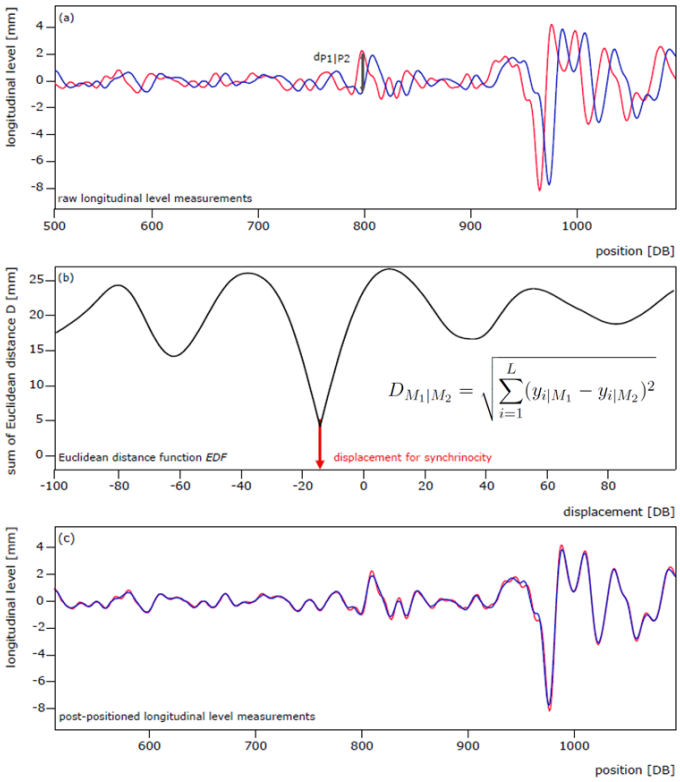

Figure 3 - Core principle of data positioning [1]

Measurement signals from different measurement runs are longitudinally shifted to each other as shown in the upper third of Figure 3. In order to obtain the necessary displacement to compensate for this offset, the two signals are gradually shifted towards each other and the Euclidean distance between the signals is calculated (middle third). The shift according to the minimum of the Euclidean distance is thus applied to synchronise the signals to each other (lower third). This procedure must be repeated for all measurement runs and for all relevant signals in order to obtain the relative positioning accuracy desired. Additionally, it must be ensured that the various measurement channels within a measurement run are synchronised to each other. Since this is not the case with the raw data, the positioning algorithm also contains respective sequences. In the last step, in addition to the relative positioning accuracy, the absolute positioning accuracy must also be considered in order to be able to pinpoint the individual signal characteristics to the respective turnout areas. For this purpose, a characteristic signal deflection of the half-gauge according to the frog gap is used in connection with the technical drawing of the turnout. Although basically already implemented, we had to adapt the algorithm in order to meet the requirements of the project. The first adaptation concerns the rail surface signal, which is not included in the original version of the algorithm and has to be treated differently due to the high sampling rate. The second adjustment corresponds to an automation of the algorithm, which is necessary in order to be able to consider a significant number of turnouts within this project.

For the rail surface signal, it has proven useful to filter it before further processing and thus remove very high-frequency components of the signal. The positioning information of the filtered signal can be transferred to the raw signal after the process, so that it is also available in a positioned form. Due to the significantly higher sampling rate of the rail surface signal compared to other data of the track measurement car, the described positioning process cannot be implemented with respect to computing performance. For this reason, we have developed a two-stage process, in which a rough positioning is carried out in the first step on the basis of the signal loss at the frog gap and in the second step the shifting is carried out by means of the Euclidian distance (with reduced shifting distance). Figure 4 shows the positioning quality before and after this procedure.

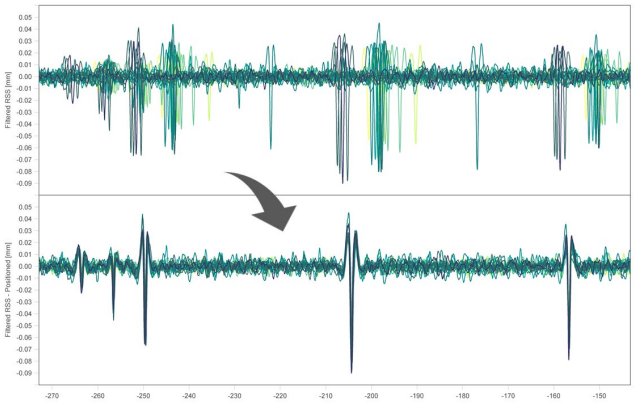

Figure 4 - RSS -Signal before and after the positioning process

By automatizing the positioning process, it is possible to significantly reduce the time required to prepare the data of a turnout (factor 10) and thus ensure that a relevant number of turnouts can be included in the evaluation. Thereby, the positioning of the longitudinal level (and thus the alignment) is carried out by means of an iterative procedure. This is necessary, because it cannot be assumed, that the correlation will deliver reliable results for a random chosen area of the turnout (signal failures of individual measurement runs, maintenance activities that have a strong effect on the signal characteristics). In the raw form of the algorithm, a window was therefore selected visually and subsequently the positioning was checked and adjusted with the help of manual control sequences. This process is very time-consuming and, due to automation, was replaced with a loop function. First, a criterion is introduced for which the positioning can be considered successful. This criterion states that the error of the relative positioning (in DB) summed over all measurement runs must not exceed a limit value. The step-by-step correlation between the measurement runs is subsequently carried out over a correlation window of width 700 DB. The signals are shifted accordingly and the quality of the correlation is checked. If the previously defined criterion is met, the loop is completed. If the criterion is not met, the correlation window is shifted 100 DB to the right and the calculation is repeated until the criterion is met. If the end of the data set is reached without the criterion being met, the criterion is increased, i.e. a worse correlation is allowed, and the correlation window is moved back to the beginning of the data set. This process is repeated until the variable criterion is fulfilled. This ensures that the relative positioning is done according to a stable subsection without having to define the window manually. The final adapted positioning algorithm includes following sequences.

Table 2 - Sequences of positioning

Sequence	Purpose
00_start sequence	Sequence in which all soft-specific settings are made and in which all other sequences are called up in the correct order.
01_Load_Data	Loading the measurement data according to the entries in 00.
02_Load_RSS	Loading the RSS data.
03_Remove_measurement_runs	Remove all erroneous measurement runs (no data, wrong track, diverging route of turnout...)
04_Sampling_Rate_ RSS	The sampling rate of the RSS signal (5 mm) is adjusted so that the signal is comparable to the other signals.
05_Load_Metadata	Metadata is loaded.
06_Preshift_LL	Shifting the longitudinal height according to the carriage position - see [1]
07_Cut_of_Signals	Prevents potential errors during mirroring.
08_Mirroring_of_measure-ment_runs	Compensation of the measuring direction.
09_Shift_Half_gauge_Reference	The half-track width of the reference run is shifted so that the practical frog tip comes to lie at 0.
09_Z_pre_shift_kilometer	The kilometre information contained in the metadata is used for an initial pre-poistioning. With this, major inaccuracies (>10m) can usually be re-moved. At the same time, the signal length is reduced from 6000 db to 4000 db after the process.
10_1_Positioning_LL_left_back	Calculation of the relative displacements of the longitudinal level between the individual measurement runs, but only for measurement runs that are older than the reference.
10_2_ Positioning _LL_left_for-ward	See 10_1, however, for measurement runs that are younger than the refer-ence measurement run.
10_3_Shift_to_frog	Shift between alignment and half-gauge.
11_1_displacement_LL_left_rela-tive	Relative displacement of all longitudinal level signals (D1) of the left side to each other. The displacements calculated in 10_1 and 10_2 are applied.
11_2_displacement_LL_left_ab-solute	Absolute displacements of the synchronous longitudinal level signals of the left side so that these coincide with the half-gauge (and thus the frog posi-tion).
12_Check_Positioning	Checks the synchronicity of the longitudinal level signals. This sequence is required for automated positioning to quantify the quality of the stationing.
13_conventional_signals_shift	The longitudinal level of the right rail, the two alignment signals and the RSS signals are shifted based on the obtained position information of the longitudinal level.
14_assign_areas	The position of the theoretical turnout tip is recognised on the basis of the signal characteristics and relevant turnout area (start, end, joints,...) are defined according to the turnout dimensions stored in the code.
15_ RSS _prepositioning	Based on the signal failure at the frog gap, the RSS signal is roughly pre-stationed.
15_Z_Corrections_Prepositioning	Generally commented out. If sequence 15 provides erroneous displace-ments, this sequence offers the possibility to do the rough stationing manu-ally.
16_ RSS_precise_positioning	The exact relative stationing of the RSS signal is determined by means of correlation.
17_Positioning_RSS_to_others	The position of the frog tip is detected in the RSS signal and all RSS signals are shifted in the following way so that they are synchronous with longitudi-nal level and alignment.
18_delete_rest	Delete all intermediate variables that are no longer needed.
19_Special shifts	Generally commented out. With this sequence, it is possible to compensate for errors in the positioning of the Longitudinal level.
20_Special_shifts_RSS	Generally commented out. With this sequence there is the possibility to compensate for errors in the positioning of the RSS.
21_Shift_Remainder	Shifting of signals for which an approximate positioning is sufficient, accord-ing to the position information of the LL. (ABA, radius, kilometre, VZG, gauge, half-gauge,…).

The positioning methodology is based on ÖBB's existing data structure and the measuring car's measuring channel specifications. If further or other data are to be included, the methodology must be adapted accordingly. This could be necessary, for example, when comparing the descriptive evaluation with acceleration data of other vehicles.

2.2 Condition assessment of frogs

Since turnouts enable the transition between two tracks, there must inevitably be a point where two rails intersect. At this point, technical measures in the form of a frog are necessary to guarantee a safe crossing. A distinction can be made between rigid frogs and movable frogs, the former scores with its simplicity (no movable components) and thus with the relatively low costs, but is associated with a gap in the running edge. Wheels react to this gap and additional dynamic forces arise in the system which in turn cause damage to the track and the vehicle. With the movable frog, there is continuous wheel-rail contact, therefore these frog types are used on high-speed lines. In Austria, rigid frogs are installed in the majority of the network, which is why they are primarily considered in this project.

Due to its complexity, it is difficult to assess the condition of the frog according to a single data source or a single quality parameter. Since the descriptive approach is based on data that is historically available and is expected to be available network-wide in the future, only this data is integrated into considerations. In the course of the project, six quality indices have emerged, which can contribute to the condition assessment of turnout crossings. The individual approaches are consequently described in detail.

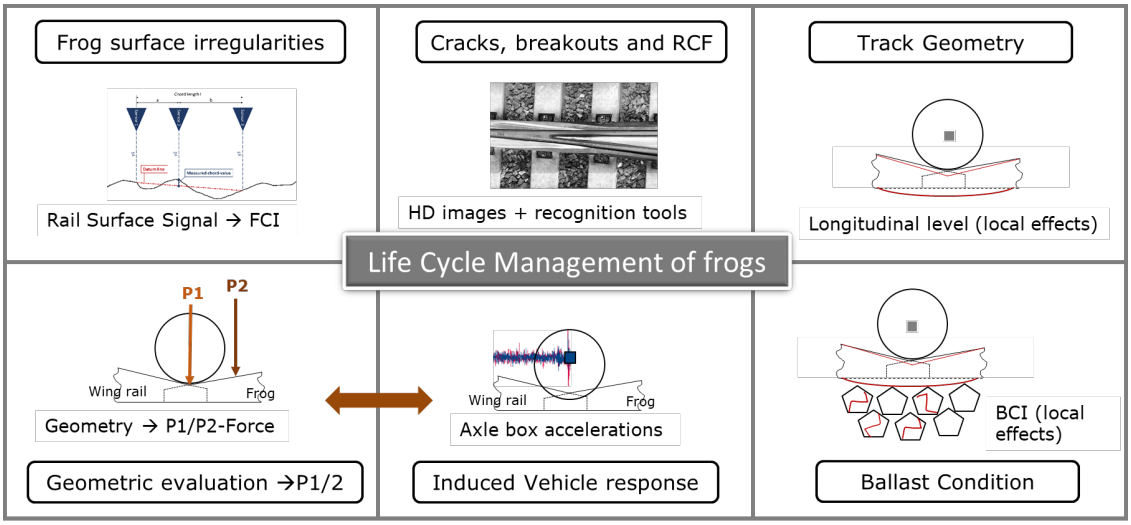

Figure 5 - Approaches for the condition assessment of frogs

2.2.1 Frog surface irregularities

The basic idea of this quality indicator is that the condition of the frog can be described according to a surface measurement of the rail. For this purpose, data from the rail surface measuring system installed on the EM250 is used. The measuring principle of the system is described in detail in report D2.2.2 Report of Requirements. The sampling rate of 5 mm allows detailed representation of the rail surface. As the measuring system only contains

short wavelengths, short-wave surface effects of the frog are measured; unevenness, as in the case of track geometry irregularities, are not detected. Since the wheel-rail contact reacts strongly to these short-wave irregularities, it is assumed that a quality index can be derived from the data, which correlates strongly with maintenance requirements.

2.2.1.1 Measuring range and data plausibility

Given that the measurement is a line-based measurement, it is necessary to analyse in advance which areas of the frog are included in the data (Figure 6).

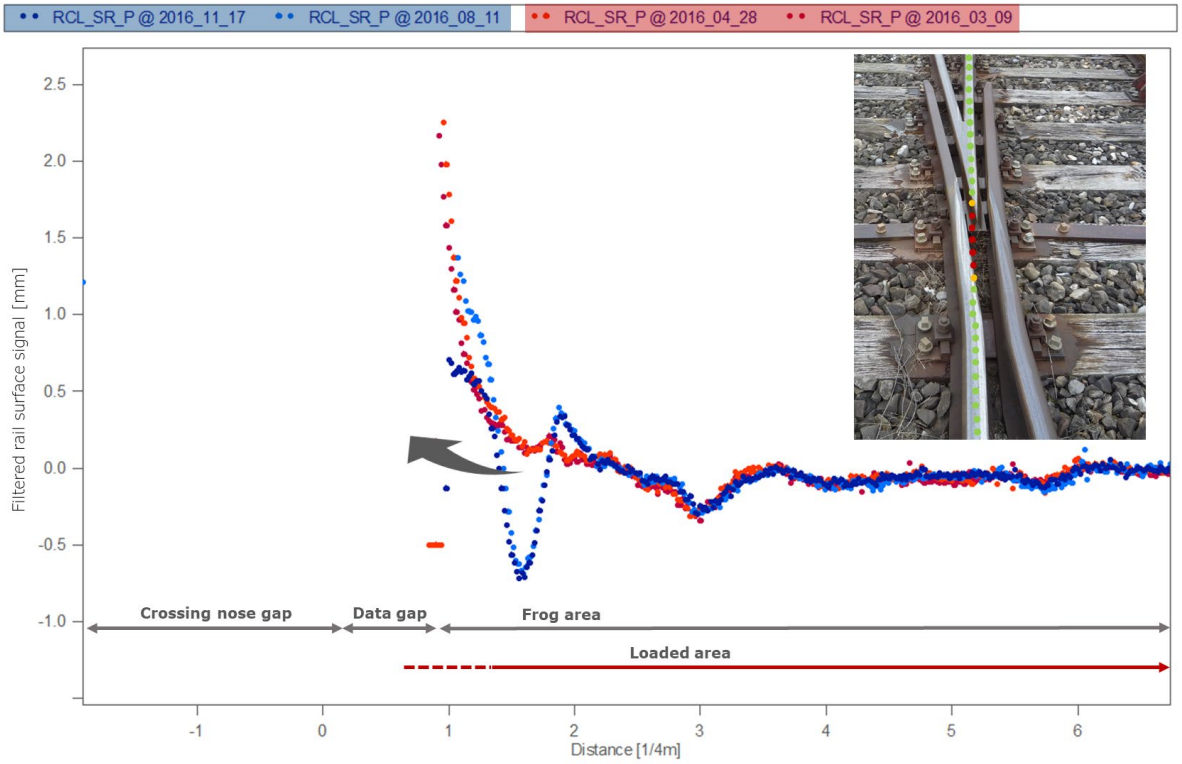

Figure 6 - Measurement range within the frog area

Three vertical lasers are aligned according to an actuator so that they always measure the centre of the rail head. The actuator is coupled with the simultaneously measured half-gauge and the sensors are aligned according to this measurement. The lateral alignment is carried out with a correspondingly high frequency. It should be noted that the system in Austria is calibrated for the 60E1 rail, so for other rail profiles there is an offset to the centre line. It is assumed that this has no significant influence on the measurement. In the frog area however, the crossing nose gap and the deviation of the frog geometry from a standard profile result in an undefined measuring range. This causes a measurement loss at the crossing nose gap (see figure). Since at this position, the half-gauge measurements also provide incorrect values, the system requires a run-in phase after the crossing nose gap (frog or wing rail). This area is labelled as "data gap" in the figure and can vary slightly

in length for the measurement runs. The tip of the frog can therefore not be detected by the measuring system. Since the tip is installed in a lowered position and is untouched by the wheel (the wheel contact point is about 200 mm later), this data gap can be accepted as long as the area does not exceed 200 mm. Whether this is the case is difficult to prove. One approximation that speaks for a sufficiently large measurement range is that the measurement results are equivalent for trailing and facing runs. In the case of trailing runs, the signal failure due to the frog gap extends after the frog, so in principle it can be assumed that the signal failure only occurs when the wheel has left the frog. If this is the case, the most exposed area of the frog is included in the data in any case. Since it can be seen that the facing run provides a similar measuring range, it can be assumed that the measuring range is also sufficient here.

The question of the exact measurement path is even more difficult to answer. This depends on the centration of the measuring system according to the half-gauge and is not reproducible at the current state of knowledge. However, there is much to suggest that the measurement path follows a similar course for each transition. This can be seen in the signal characteristics in Figure 6. The two blue measurements and the two red measurements each describe measurement runs that are close to each other in time, where the condition of the frog can be considered similar. The signal characteristics are also similar here, the measurement is therefore stable. This can also be confirmed by other examples. A clear change in the signal characteristics can be seen between the red and the blue measurements. This can be explained by a maintenance operation that was carried out (and documented) here.

In summary, the measurements of the rail surface measurement system, although not designed for the frog area, seem to provide useful data for an evaluation index. Consequently, the calculations of this are described.

2.2.1.2 Definition of a quality index – Rail surface signal

In order to automate the index calculation, the exact localisation of the frog (considering measurement losses of different runs) must also be automated. For this, a distinction must be made between frog and frog gap as well as frog and open track, whereby the former can have a significant influence on the calculated index. Data gaps are represented as infinite values, but also the first measured data points may partly not be taken into account, because they are still falsified due to the chord measurement principle (one of the sensors is still located in the frog gap). The classification of the data takes advantage of the fact that the measuring system maintains the level of the last actually measured point for 20 measuring points after a measuring failure (see Figure 7)

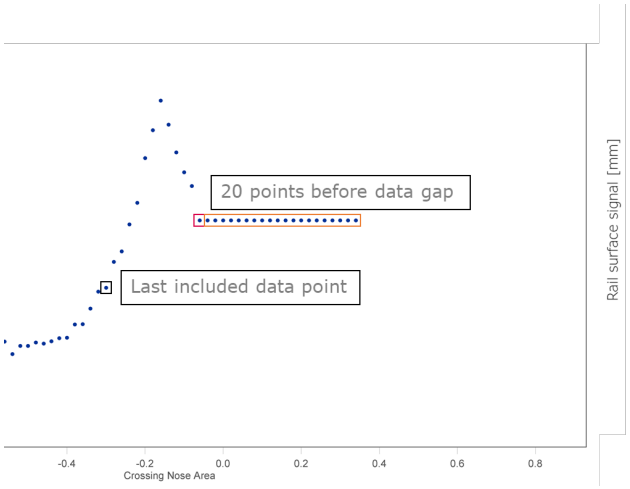

Figure 7 - Detailed signal analysis near the data gap

By calculating the standard deviation over 20 data points, it is possible to detect this section automatically. If further data point specific queries are carried out, the first point that fulfils these queries can be defined as the first regular measuring point of the frog (in this case on the left of the data gap). If the data are now additionally intersected with the dimensions of the frog according to the construction plan, the last data point in the frog area can also be defined. This was defined in such a way that the connection weld of the frog is still completely included in the data.

Now that the data classification can be automatically emitted, the next step is to actually calculate a quality index. First attempts to use the raw data of the RSS signal were unsuccessful. Among other issues, extreme values, standard deviations and frequency evaluations were examined as potential index values. Currently, the following method appears to be the best option:

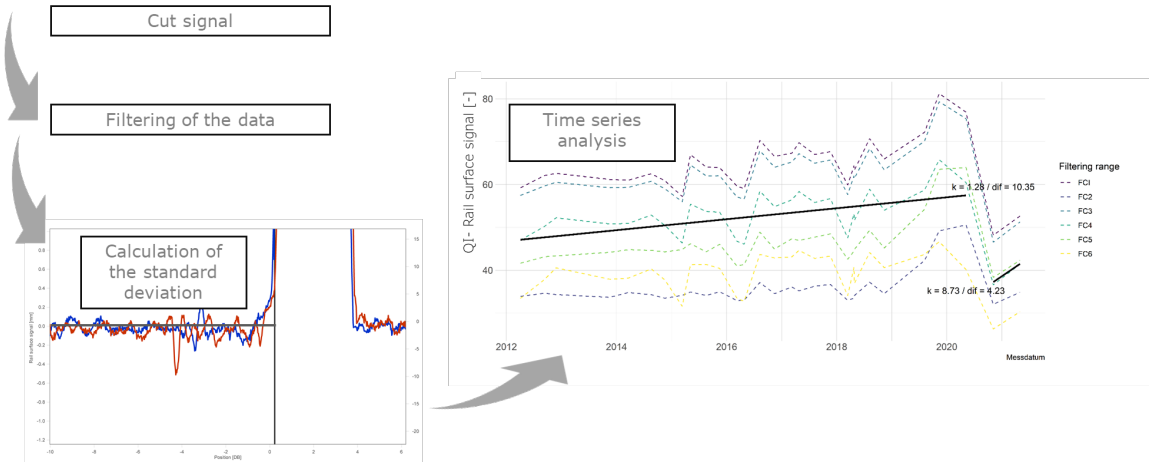

Figure 8 - Work flow for quality index extraction - RSS

After the relevant data has been extracted, the data is filtered. Currently, 6 frequency ranges of the filtering are under observation. The significance of the individual frequency ranges will be verified with historical maintenance activities. The filtering is done using bandpass filtering without phase shift (Butterworth, 4th order) and according to the threshold frequencies (wavelengths) from Table 3. Consequently, the standard deviation is calculated for the 6 signal sections. The standard deviation reflects the noise of the signals, high values thus indicate unevenness in the respective wavelength range. Once this calculation has been completed, the index determined can be observed over time and checked for its plausibility.

Table 3 - Filtering ranges

Filtering range 1	0,1 m – 0,4 m
Filtering range 2	0,05 m – 0,15 m
Filtering range 3	0,1 m – 0,35 m
Filtering range 4	0,15 m – 0,3 m
Filtering range 5	0,1 m – 0,2 m
Filtering range 5	0,2 m – 0,3 m

The development of the index over time is for now approximated with a linear regression in order to show the deterioration over time. From this, characteristic values of the slope and the absolute deterioration of a deterioration branch can be calculated. As the example in Figure 8 shows, the maintenance input documented for 2021 can be seen in the development over time for all filter classes. A fundamental deterioration over time is also evident, which corresponds to the expectations of the quality behaviour. It can be deduced that the calculated index is related to reality and that further evaluations are recommended.

2.2.1.3 Index plausibility check

For the plausibility check of the calculated index, we analysed the development over time of the 30 project turnouts (with partly several significant deterioration branches). This results into 40 deterioration branches, which can be classified into 4 categories (Figure 9).

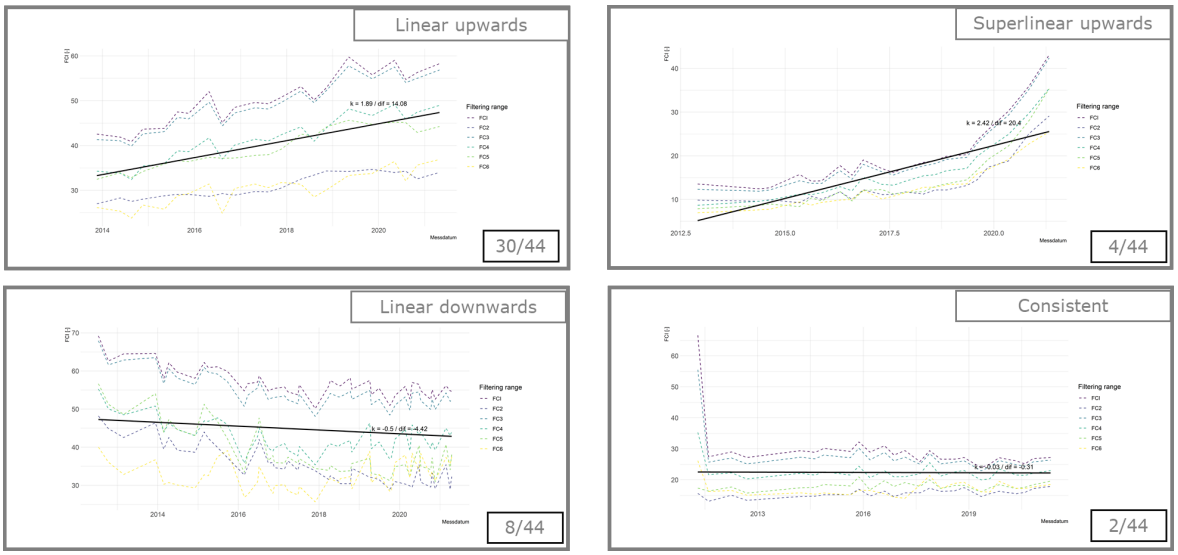

Figure 9 - Classification of deterioration behaviours

It can be concluded that 8 out of 10 deterioration branches show an upward trend. About 2 out of 10 deterioration branches show a unified downward trend, and only 2 of the 44 deterioration branches show a stagnating level within the index. Although there are outliers, most of the developments are in line with expectations in terms of the development of the trend over time. It can also not be completely ruled out that the corrugation of the rail surface decreases in some frogs due to wear. Assuming that this is the case, i.e. that the negative development over time is a plausible case, and correlating the slopes of the 44 deterioration branches with the documented daily tonnage of the frog, a p-value of 0.0047 results. With the usual significance threshold of 0.05, it can therefore be statistically proven that a correlation exists between the slopes of the deterioration branches and the daily tonnage, which is equivalent to the statement that the index changes more quickly with higher loads.

The index therefore seems to allow statistical statements about the condition of the frog, but some uncertainties remain. In contrast to the development over time, the absolute value of the index does not show any correlation with the condition of the frog. Currently, two frogs cannot be compared with each other according to the index, only the analysis of the behaviour over time is possible. Under these boundary conditions, it will be difficult to establish a limit value at a later stage of the project. It is assumed that a frog should be exchanged as soon as the development over time enters the over-linear range, but more frogs have to be investigated for validation. Another issue could be, that the index is strongly influenced by the welding between the frog and the rail. It cannot yet be answered whether this strong influence includes unwanted effects in the condition assessment.

2.2.1.4 Examples of index behaviour (rail surface)

Three typical examples of the development of the rail surface index over time will be discussed here. These examples were also chosen because at least one frog exchange is known according to the available documentation. The data basis basically goes back to 2005, but data before the renewal of a turnout is not taken into account. This is the reason why the time series of turnout T_R4F_05 (Figure 10) starts in 2014.

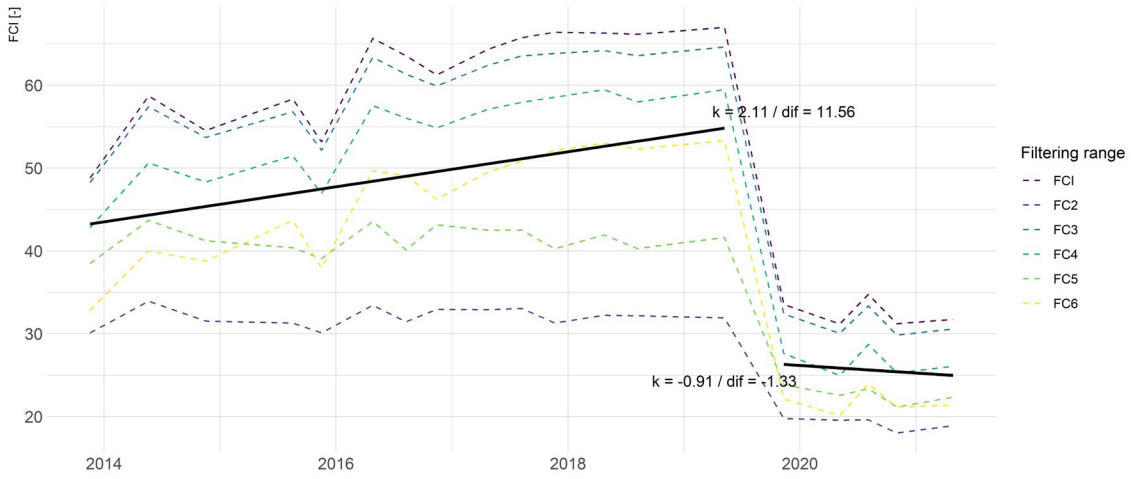

Figure 10 - Rail surface index - T_R4F_05

The index behaves as expected. The deterioration branch between 2014 and 2019 shows a linear trend with no significant outliers. As a result of the frog exchange in 2019, there is a significant drop visible within the time series of the index, a good frog condition after the exchange can be confirmed. After the exchange, the quality has been practically constant respectively slightly downward. This trend can be seen in many of the project turnouts considered. After a corresponding period of time, the trend usually reverses (not yet visible in this example). One explanation for this could be the "running-in" of the system (especially in the case of manganese frogs). A basically similar behaviour, but with clear outliers, can be observed with the turnout from Figure 11.

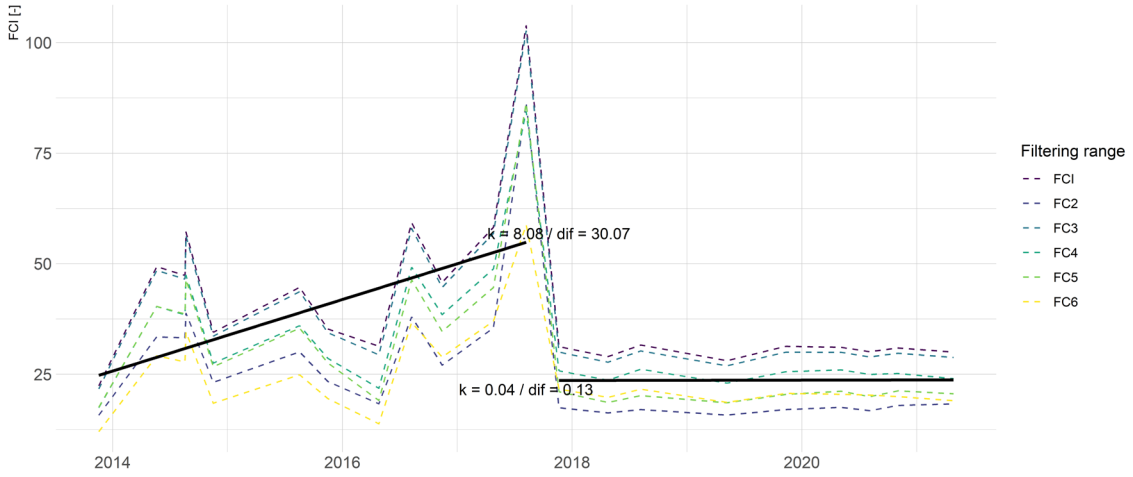

Figure 11 - Rail surface index - T_R4F_08

Here, too, there is an upward trend in the first deterioration branch, but in an over-linear form and with clear outliers. These are explained due to the data quality. The frog exchange in 2017 is associated with a clear drop of the index, so the exchange is again visible within the index. The quality behaviour after the frog exchange can be described as unusual; the index rameins at the same very low level since 2017. Whether this is a case of a high-quality frog under favourable conditions or whether the index delivers incorrect values is part of future analyses. A not easily explainable behaviour of the index is contained in the example in Figure 12.

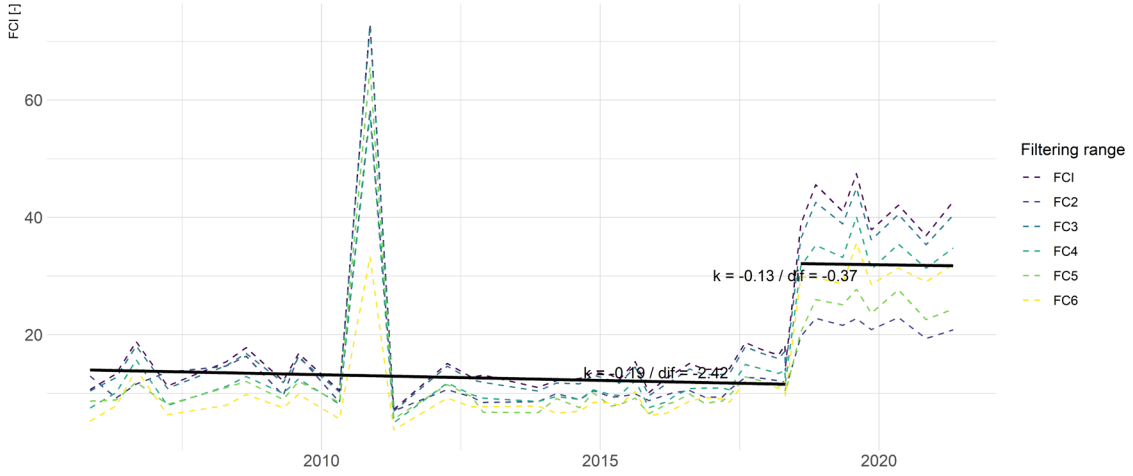

Figure 12 - Rail surface index - T_R4F_24

The characteristic highlights two major problems of the index. There is negative deterioration over the entire observation, which corresponds to a reduction of the corrugation over time. As already described, it cannot be completely ruled out that this circumstance corresponds to reality, but it definitely complicates the interpretation of the index. The outlier in 2010 does not pose any significant problems. A much bigger problem is the behaviour

due to the frog exchange in 2018. Here, the index does not drop downwards, as expected, but rises. The corrugation of the rail surface due to the new frog is therefore higher than with the old one. If this corresponds to reality, it is difficult to make comparisons between different frogs, as already described. If the initial level of the new frog after the exchange coincidentally corresponds to the final level of the old frog, an exchange of frogs can be completely overlooked.

It should be added that this is an extreme example, but it raises many questions about the index validity. These questions require further considerations; however, it can be assumed that in principle information about a partial aspect of the frog condition can be derived from the rail surface signal. As described in 2.2, the description of the condition of the frog - based on available data - can only be done according to the consideration of several indicators.

2.2.2 Cracks, breakouts and RCF

Due to the measurement characteristics of the RSS measurement system, cracks cannot be detected analysing this signal. Also, break-outs and RCF appearances are only recorded in the signal if they are "coincidentally" located in the measuring range of the measuring system. For these reasons, the effects mentioned must be evaluated using a different data source. One possibility for this is the HD camera system that has been installed on the measuring car EM250 since 2020. Image material is stored for each measurement run, Figure 13 shows the frog of one of the project turnouts.

Figure 13 - Frog of one of the project turnouts

Although there is already a high level of wear in the transition area, there are no cracks, break-outs or signs of fatigue to be seen. Currently, these images can only be evaluated visually. If other parameters show abnormalities, HD images can be used for verification. In the long term, it is expected that the detection of undesirable phenomena will be done by means of image recognition tools. There are already many approaches in the literature [2] [3], but there is still a need for research to find satisfactory solutions in terms of false-positive and false-negative rates. The development of image recognition tools of sufficient quality requires in-depth expertise and/or an extended time horizon and is therefore not pursued further within this project. However, we can use the HD images to verify the deflections of the rail surface signal respectively the classification of the deflections. Due to the very similar structure of turnouts (switch panel, closure panel and crossing panel), these are similar for each turnout in their relative position.

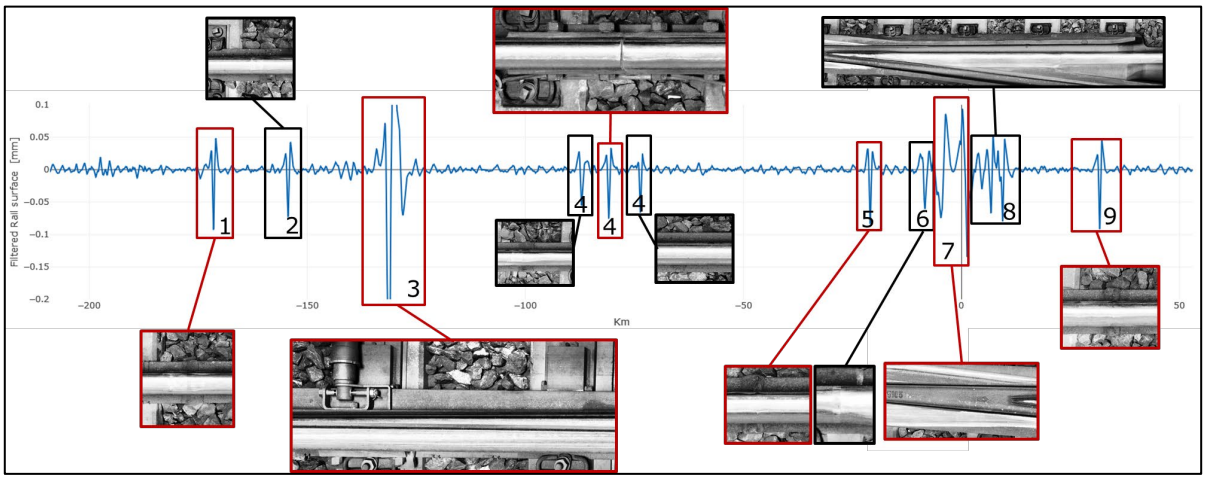

Figure 14 - Verification of classification of RSS deflections

Essentially, the arrangement of signal deflections in Figure 5 is the same for each turnout. The deflections 1 and 2 occur as a result of welded joints, whereby deflection 1 does not actually belong to this turnout, but to the downstream turnout not included in the figure. Therefore, the welding joint connecting the open track and the switch panel is located at deflection 2. The HD pictures confirm that there are actually two welding joints. Deflection 3 occurs due to the transition from the stock rail to the switch rail and is to be understood as a signal failure that has no correlation to the actual state of the transition. The failure is due to the fact that the RSS system is coupled with the measurement of the half gauge (lateral positioning of the sensors) and the measurement of the half gauge includes a systematic failure at this position. Deflection 4 reflects the transition between switch panel and closure panel and is designed as an insulated rail joint. It should be noted that there are differences between the turnouts as to which connection is designed as an insulated rail joint and which as a welding joint. These can also be interchanged (2 = insulated rail joint and 4 = welded joint). In this case, 4 is an insulated rail joint, which can be clearly seen in the signal characteristics. This includes three deflections, whereby the two outer deflections occur as a result of two welds and the middle deflection as a result of the insulating spot. The HD images confirm, that it is an insulated rail joint. 5 and 9 again show two welding joints, 5 reflects the transition between the closure panel and the crossing panel and 9 the transition between the crossing panel and the open track. Point 6 shows the three-metal welding of the frog, which is necessary because manganese hearts cannot be welded outside the manufacturing hall. This welding can also be seen at the end of point 8. The heart itself is visible in 8, which follows the frog gap (7). After all classifications of the signal deflections of the RSS signal could be verified by means of HD images, a condition assessment of the significant points can be intensified by means of the RSS signal. This is detailed explained in 2.3.

2.2.3 Track Geometry within the frog area

Single failures of the track geometry often occur at typical spots within turnouts. These are in the transition area between the open track and the turnout (stiffness transition, sometimes also different rail profiles), beneath insulated rail joints and welding joints (dynamic load input) as well as in the crossing area (dynamic load input). Figure 15 shows a turnout where each of the described spots are visible.

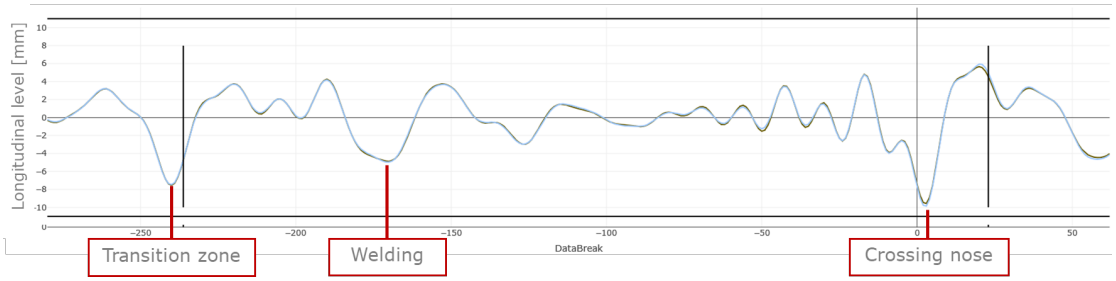

Figure 15 - Longitudinal level within turnout P_W_13

Naturally, the extent the failures vary for different turnouts and is highly dependent on the age of the system, traffic and the quality of the components installed (including subsoil and ballast). For the example shown, single failures close to the alert limit can already be detected in the transition zone and in the crossing area. Although the analysis of all these effects is of interest, only the at the point of the frog is pursued in this part of the report, in accordance with the aim of describing the condition of the frog. Two thirds of the 30 project turnouts show at least once a single failure at the position of the frog with more than 4 mm since 2005. About one third even with more than 6 mm. Since the project turnouts are equipped with monitored experimental frogs, it is assumed that above-average care was taken with the bedding of the frogs and that the net-wide average is somewhat poorer.

The track geometry at the location of the frog does not give any information about the condition of the frog itself, but very much about the bedding conditions in the frog area. If, for example, increased dynamic forces due to the crossing can be detected, it is basically not known why these occur. The vehicle reacts on both, a bad condition of the frog itself (wear, breakouts,...) and to unevenness due to local settlements of the track grid (track geometry). Thus, considering a track geometry failure in the area of the frog, a more substantiated assessment of necessary maintenance activities can be made.

Figure 16 shows the time series of the maximum amplitude of the single failure of the track geometry within the crossing area of one of the project turnouts. The turnout was renewed in 2012, so the time series does not go back further.

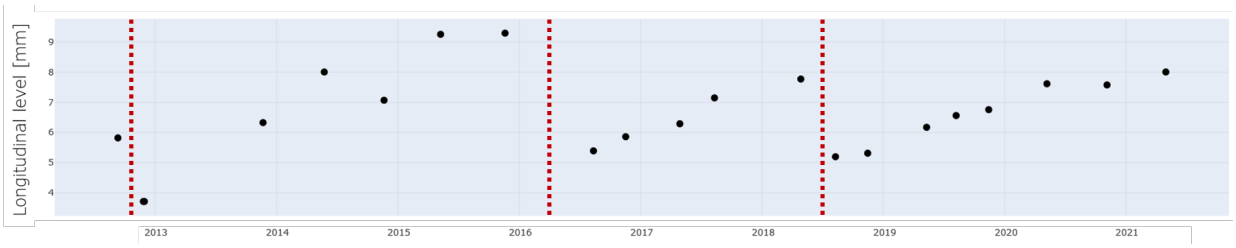

Figure 16 - Single failure of track geometry - time series

Basically, two core statements can be derived from the figure: 1) The time series is stable and behaves similarly to single failures of the open track. 2) The single failure can reach very severe levels and, at 9 mm, is already close to the alert limit in this case. Without the necessary maintenance, a safety-critical level would be reached relatively quickly. Historic tamping actions are not known for this turnout, but they can nevertheless be clearly identified from the data (red vertical lines). Outliers, like the one at the end of 2014, can be classified using the raw signal.

The basic procedure for frog exchanges is bringing the ballast under the frog to its nominal position and thus ensuring a good bedding for the new crossing. However, the data evaluation shows that this is not always the case. The two extreme cases are depicted in Figure 17.

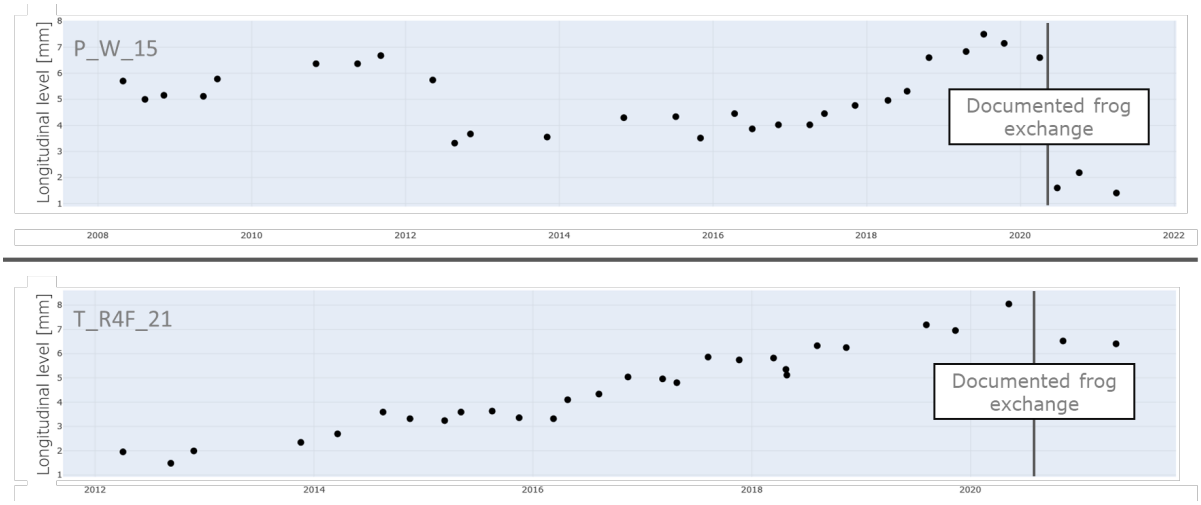

Figure 17 - Track geometry before/after frog renewal

The development over time of the quality parameter in the frog area is shown for two turnouts. For both turnouts, according to information from the responsible staff, a frog exchange can be assumed in 2021. While a clear improvement in the track geometry is recorded for the turnout with the identifier P_W_15, the track geometry remains practically at the same poor level for turnout T_R4F_21 after the frog exchange. It can be assumed, that this has a significant influence on the further development of the frog condition and

that higher dynamic forces act on the frog of turnout T_R4F_21, until the failure will be corrected.

There are considerations about the reliability of the longitudinal level in the frog area by means of inertial measurement. In principle, the longitudinal level measurement is carried out by acceleration sensors, which record the acceleration of the measuring frame as well as data processing (filtering, double integration, ...) in order to obtain the relative space curve of the track geometry. The wheelset under the measuring frame experiences accelerations due to the frog geometry, additionally to the accelerations due to actual track geometry. The signal thereafter basically gets integrated and filtered (D1, D2). In principle, due to this filter process, the measured effect from the frog geometry should be neglected, but filters do not work keenly in border areas. Therefore, it cannot be completely rejected that the longitudinal level data is influenced by the frog geometry and therefore does not reflect the track geometry alone. However, some points still count for a reliable measurement:

- The longitudinal level (D1) includes wavelengths of 3-25m and the frog geometry is expected to include much shorter wavelength. While the D0 range of longitudinal level is clearly influenced by this effect, the effect on the D1 range should be relatively small (see filter characteristics with relatively sharp declines at low wavelengths in [4])
- The time series of the track geometry is stable.
- Partially, the single failure remains even after a frog exchange (see Figure 17). If the track geometry measurement was strongly influenced by the condition of the frog itself, the single failure would have to decrease strongly with each frog exchange.

Nevertheless, this aspect will be further investigated in the course of the project. For this purpose, the correlation between the index value according to the track geometry and the index value according to the axle box acceleration will be analysed. It is also intended to compare the longitudinal level measurement according to the IMU with chord measurements. Due to the different measuring principle, it is expected that chord measurements correctly record the track geometry at the frog of the turnout. Chord measurements of track geometry are only performed by construction machinery in Austria nowadays. A data request has already been made in this regard.

2.2.4 Ballast condition within the frog area

In addition to track geometry, the condition of the ballast beneath the frog has a significant influence on the quality behaviour of the system. If a corresponding proportion of the ballast is pulverised and contained as fine particles in the ballast bed, the stiffness in the system is correspondingly increased, the load transfer can no longer take place as intended and additional system forces lead to increased component stress. It has not yet been possible to investigate how this relationship affects the frog, but it can be assumed that the effects of poor ballast condition act negatively. Indirectly, there is a negative effect, as the poor condition of the ballast leads to problems in track geometry, which in turn has a negative influence on the quality behaviour of the frog. The first step for further research on this relationship is to characterise the condition of the ballast. Here Fellinger [1] developed a method according to which classification is possible by means of longitudinal level measurements. The Ballast Condition Index (BCI) is based on the fact that different wavelength components of the track geometry are caused by problems of different components. If only the proportions that arise due to poor ballast condition are considered, conclusions can be drawn about the quality of the ballast. As shown in Figure 18, the characteristic value calculation is carried out according to the power density spectrum of the longitudinal level measurements.

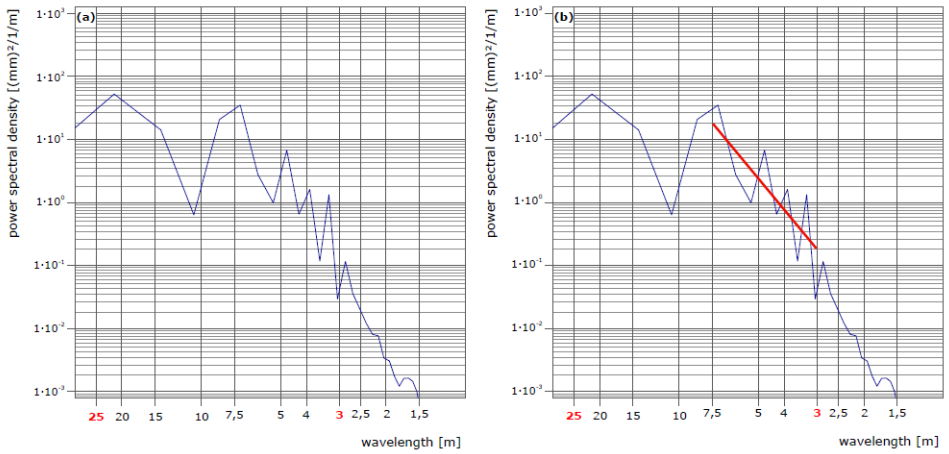

Figure 18 - Ballast Condition Index - PDS curves [1]

The left side of the figure shows the power density spectrum, determined from the longitudinal level (D1) calculated over the entire length of the turnout. As in the railway infrastructure sector we usually refer to wavelengths, these are plotted on the x-axis instead of the more common frequencies. The BCI is subsequently calculated from the slope of the regression line in the range between 3 and 7.5 metres. The regression line can be seen on the right side of the figure. Descriptions of the characteristic value (e.g. choice of wavelength range) as well as the validation process are documented in detail in [1]. As it is

essential for the overall impression of the turnout condition, we applied the BCI to all project turnouts, Figure 19 gives an example how the index behaves over time.

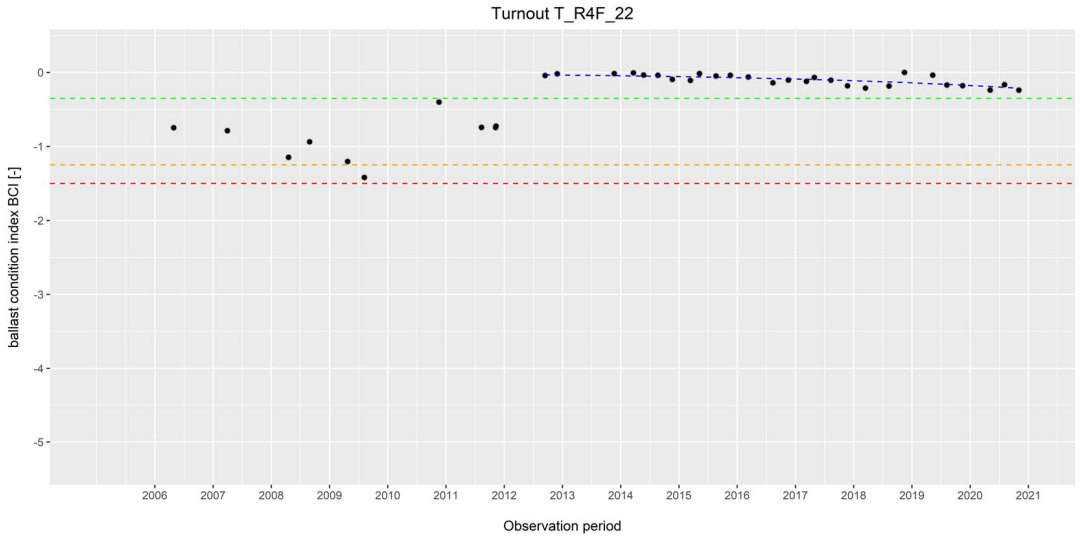

Figure 19 - Time series of BCI - example

For the turnout shown, it can be observed that there were obviously problems with the condition of the ballast before it was renewed in 2012 and that these were eliminated with the renewal (ballast replacement). Since then, the ballast has only deteriorated very slowly and is still in a very good condition in 2021. Therefore, ballast problems are not to be expected in the next 10 years.

Although this description is a good approximation, local problems of ballast quality can occur, especially in the frog area. As the described characteristic value is averaged over the entire turnout, a generally good ballast quality can mask local problems. In order to be able to evaluate these local problems of the ballast, especially in the frog area, the BCI must be calculated for partial areas of the turnout. It has already been shown that this method is fundamentally effective. The question that will be taken up in the further course of the project is how short the influence length can be chosen so that reliable results are still produced, but these can be assigned as precisely as possible to the area of the frog. Currently, it is assumed that the minimum influence length is the upper end of the considered wavelengths, i.e. 7.5 metres.

2.2.5 Vehicle reactions caused by frog transitions

The purpose of infrastructure is to ensure a smooth vehicle pass. If track components are in a condition that causes stimulations of the vehicle, additional dynamic forces are generated within the system leading to a higher deterioration of the system. In the frog area (in

rigid design), increased force effects are unavoidable due to the geometric boundary conditions. In the transition area between the wing rail and the frog, vertical excitations of the wheel as well as an increased slip inevitably occur. If these excitations are unusually high, it can be assumed that either the wheel or the frog is in an unfavourable condition. The described vertical excitations can be detected by means of axle box acceleration sensors. Among many other measuring systems, these sensors are installed on the EM250. This part of the report deals with the question, whether the acceleration data of the measuring car can be used to draw conclusions about the condition of the frog. If the answer to this question is yes, there is a great potential given, as the data is available network-wide and is regularly recorded and included in the current data structure. Compared to sensor concepts mounted onto the infrastructure, there are advantages in terms of quantity and costs, and compared to OBM solutions, there are advantages in terms of enforceability (data sovereignty, data volumes, ...). In answering this question, three problems arise, which will be addressed specifically within three subchapters.

2.2.5.1 Data characteristic of the EM250 acceleration data

The axle box acceleration data of the measuring car was originally used to detect corrugations. As corrugations have specific wavelengths the measured raw signal is filtered accordingly on the measuring car before it is stored. It has not yet been possible to determine exactly how the filters are applied, but the data excludes large parts of the wavelength spectrum. As an example, the signal for turnout P_W_13 is shown in Figure 20.

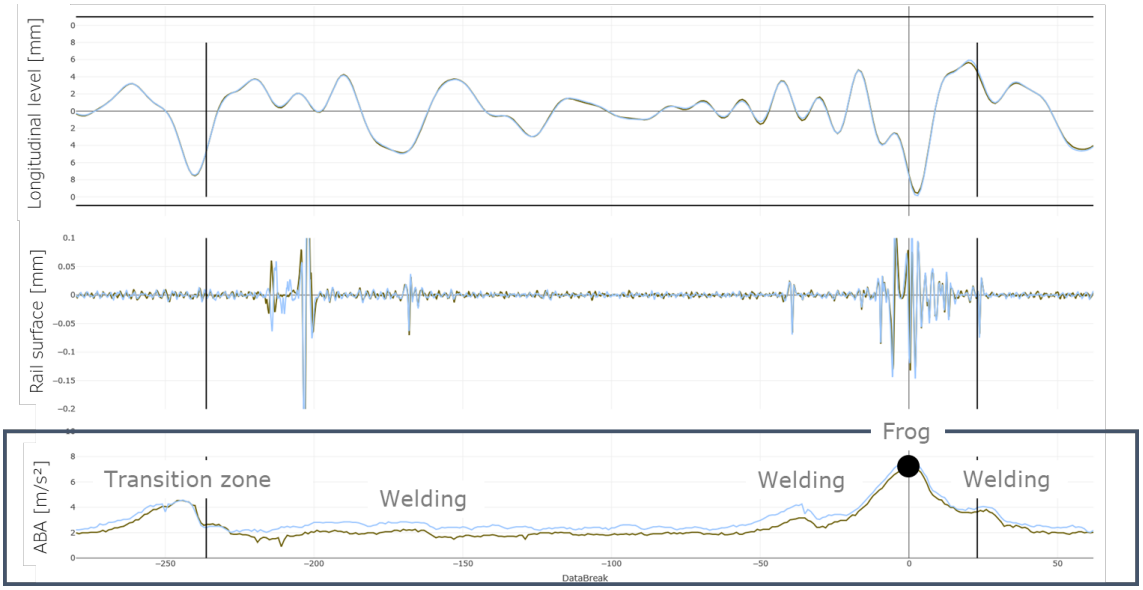

Figure 20 - Axle box acceleration within a turnout area

The turnout (including adjacent areas) covers nearly 100 metres. The axle box acceleration data is shown in the bottom third of the figure. For a better understanding, the longitudinal

level (top third) and the rail surface (middle third) are also illustrated. It can be seen that no short-wave components are included in the signal of the axle box acceleration. However, if the vehicle reacts to short-wave effects, they are visible in the signal, but in a smoothed way. This suggests that the signal is heavily smoothed and not a filtered, which means short wave-effects are not entirely removed from the characteristic, but merely blurred. Examples of this are the transition area at the beginning of the turnout (see track geometry), the three rail joints (see deflections in the RSS signal) and at the frog itself (see RSS signal and longitudinal level). Especially at the frog, a dominant deflection can be detected. This signal characteristic could also be recorded with other turnouts. It can therefore be assumed that, although not stored in its raw form, reliable information about the vehicle excitation due to the crossing of the frog is contained in the axle box acceleration (ABA) signal of the measuring car.

For the condition assessment of the frog according to the axle box acceleration data, it is necessary to derive a quality index from the data. It must be taken into account that this type of data is not included in the positioning methodology and cannot be transferred to the absolute position of the other signals by means of correlations, due to its highly smoothed form. For the further course of the project, we consider the possibility of additional post-stationing process; currently, potential inaccuracies are being taken into account in the compilation of quality index. An influence range of +-10 metres starting from the frog point is chosen for the index value calculation. On the one hand, this takes into account the potential inaccuracies of the positioning quality, on the other hand, accelerations due to the frog have an effect over a longer range anyway due to the strong smoothing of the signal. Attempts to derive the quality index according to the maximum value failed because no stable time series could be represented here. For this reason (and the validation seen later), the RMS value over the described range was introduced as the quality index.

$$QI_{ABA} = RMS(ABA_{\pm 10m})$$

In this form, however, the calculated quality index is not meaningful, as the influence of the measuring speed falsifies any assessment.

2.2.5.2 Influence of vehicle speed

Axle box accelerations as input for the condition assessment of the track have the disadvantage that the measurements depend not only on the condition of the track but also on the characteristics of the vehicle. The speed of the vehicle has a particular influence here. This relationship can be easily demonstrated if the calculated quality index and the measurement speed are compared with the corresponding scaling.

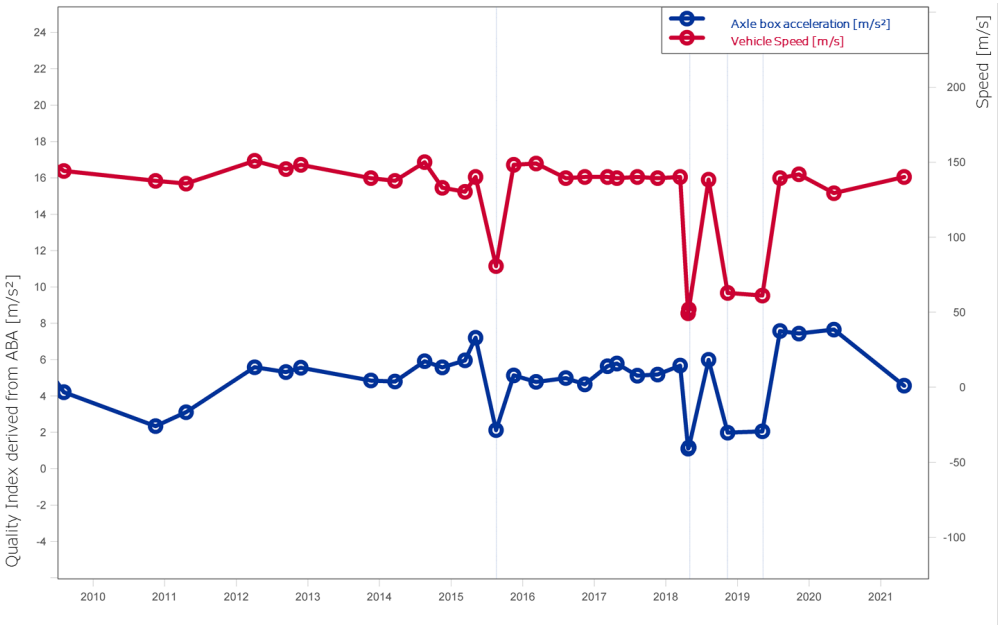

Figure 21 - Correlation between ABA and vehicle speed

The development of the ABA index over time is shown in blue, the speed of the measuring car during the frog crossing at the respective measuring run is shown in red. A clear correlation can be recognised if the crossings with lower speed are considered, here the ABA index values are also clearly lower and do not correspond to the trend of the data. This generally shows a slight increase over time, with sudden improvements in the years 2015 and 2021, thus corresponding to a system that deteriorates over time and whose condition improves suddenly as a result of maintenance measures. To remove the influence of speed from the quality index, the index must be related to the speed. An obvious way to do this is to divide the index by the respective speed. However, it turns out, that the influence of speed is underestimated according to this scaling. The influence therefore seems to be superlinear. If the index is divided by the square of the speed, the influence of the speed is overestimated. In this case, measurement runs at lower speeds result in higher index values. It can thus be concluded that in order to eliminate the influence of speed, a scaling with speed with a power between 1 and 2 must be carried out. For the exact value, we scaled the index with the speed to all powers between 1 and 2 and evaluated the result both visually and by correlating the speed with the calculated index (over time). The lowest possible correlation after scaling is desirable. This method results in a scaling factor of V^1.55. This results in the final quality index according to the axle box acceleration using:

$$QI_{ABA\_scaled} = \frac{RMS(ABA_{\pm 10m})}{V^{1,55}}$$

The speed is used here in the unit km/h, the axle box accelerations as m/s. From a physical point of view, the calculated characteristic value therefore no longer corresponds to the

unit m/s², since the unit calculated has no significance here, the characteristic value is therefore treated as unitless. In Figure 22 the curves shown in Figure 21 are extended by the scaled index value. Due to the scaling, the absolute values of the index differ greatly from the raw data.

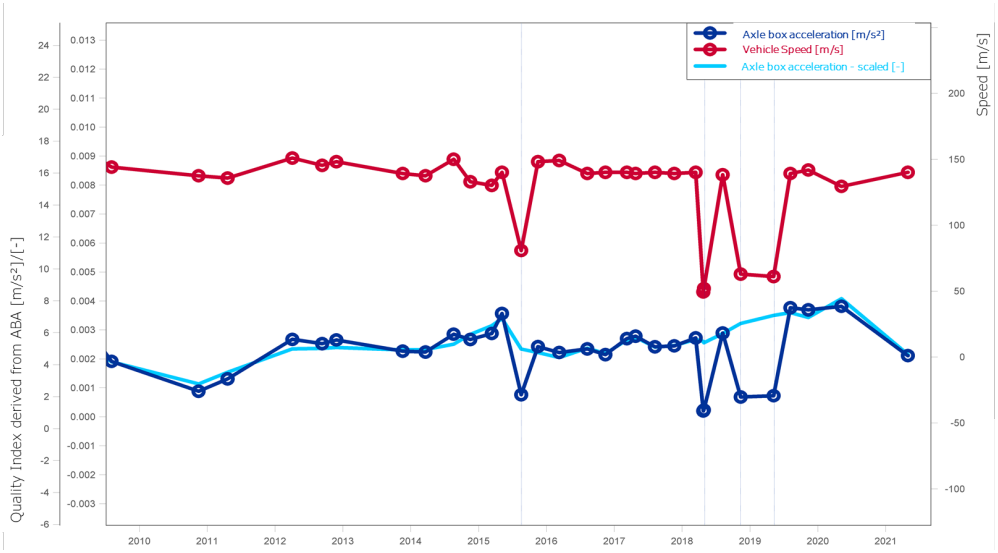

Figure 22 - Scaled quality index (ABA)

The light blue data series corresponds to the scaled index values. As can be seen, the data points are independent of the speed and describe an expected development. Other examples also show that the influence of speed could be successfully eliminated. At the current time, this method could only be tested at the basic speed level of 140 km/h, as all project turnouts are restricted to this speed level. It cannot be excluded that runs at a completely different speed level (e.g. 20 km/h or 230 km/h) have to be treated in a special way. These uncertainties will be addressed in the further course of the project.

2.2.5.3 Influence of the wheel condition

Another vehicle parameter with significantly high influence on the crossing and thus the measured axle box accelerations, is the condition of the wheels (see analyses of working group 3 - Virtual Vehicle). Although it can be assumed that the maintenance of the wheels of the measurement car is carried out in such a way that the wheels are always in good condition, an influence cannot be completely ruled out. The suggestion of the project partner (Virtual Vehicle) is that simulations are carried out both with the standard profile of the measuring car's wheels (condition after maintenance) and with the worst permitted condition (directly before maintenance). From the simulations, the range of variation of the index according to the wheel condition can be defined. It is expected that the range of variation is very small and that the wheel condition of the measuring car can be neglected due to the dense maintenance interval. If this is not the case, further considerations will

be made. The data of the wheel profiles before and after maintenance, necessary for the simulation, were requested in status meeting 6.

Consequently, some of the project turnouts will be used to show how the described index develops over time and what conclusions can be drawn from it. In principle, the index calculation and visualisation has already been automated and applied for each of the project turnouts.

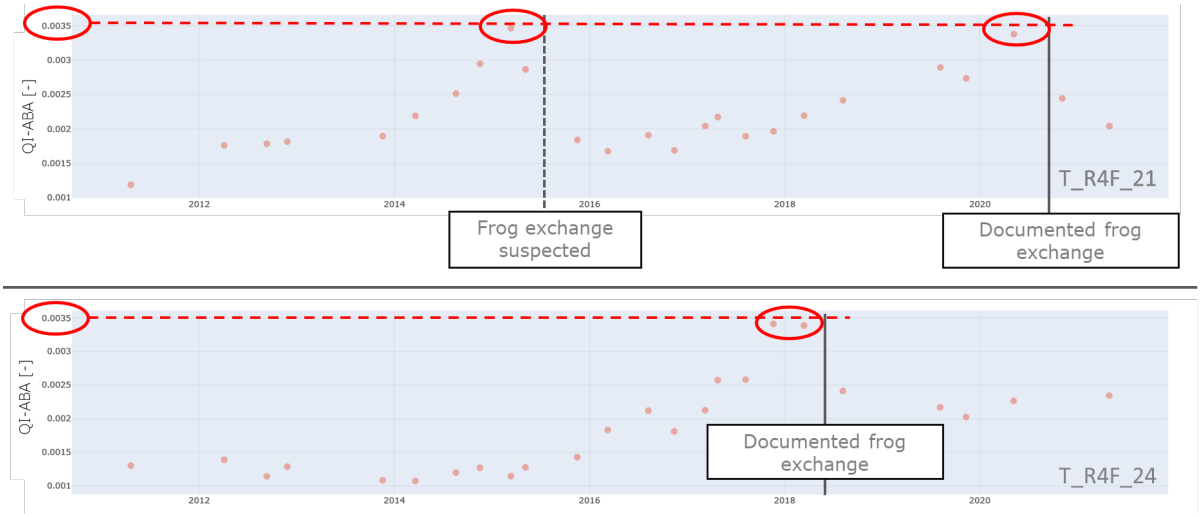

Figure 23 - Time series of quality index (ABA)

The turnouts with the identifiers T_R4F_21 and T_R4F_24, shown in Figure 23, present a similar picture. From additional sources of information, a frog exchange is known in each case (see figure). It can be seen that the calculated quality index takes on higher values over time. Thereby, the development is increasing in an overline manner. After the documented frog exchange, the index value decreases abruptly again. This development corresponds to the expectations and can be understood as confirmation that the index contains information about the condition of the frog. For the turnout T_R4F_21, it can be assumed that an additional frog exchange took place in 2015. From the signal characteristics, it can be clearly seen that the vehicle response has dropped here considerably between two measurement runs. It is noticeable that frog exchanges are often carried out near an index value of 0.35; this value is only very rarely exceeded. This circumstance can be clearly seen in the examples shown. It can be assumed that this value is associated with the "beating" of the frog. For the track engineers, this acoustic impression is indicating the need of maintenance or frog exchange. More detailed surveys and a comparison of the index with the experience of asset managers is planned in the course of the project. It can be assumed that different crossing geometries (length and inclination) lead to different vehicle reactions and thus a "limit value" of the calculated index must also be set variably. This question will also be addressed in the ongoing project. It should also be mentioned

that, although the development of the index over time corresponds to recorded measures in most cases, there is also a relevant number of outliers and, in some cases, unexplainable time series. The aim of the project is to enable for condition forecasts and to derive necessary actions. For this purpose, some open questions still need to be answered.

2.2.6 Dynamic forces due to the frog geometry

"Generally, the material response to loading can be distinguished between plastic deformation, wear or rolling contact fatigue (RCF) and all these mechanisms can lead to a worse transition geometry that demands for maintenance actions." [5] If this change in geometry can be measured, a condition assessment can be based on data. For this reason, the project turnouts were chosen due to the fact that they have already been monitored by voestalpine for several years. Geometry measurements were carried out in regular intervals using the Calipri measuring system. Details of the measurement data are already described in D2.2.2 Report of Requirements. The three-dimensional geometry calculated from the measurements with colour coding of plastic deformation (blue) and wear (red) can be seen in Figure 24.

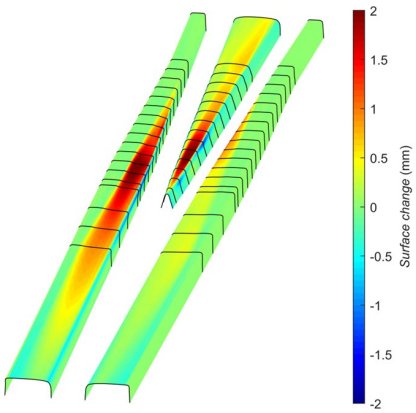

Figure 24 - Frog geometry visualisation

At the time of this measurement, the frog was under loading already for eight years and was exposed to a load of about 177 MGT. A large amount of wear can be identified, especially in the transition area, where the wheel passes from the wing rail to the frog (or vice versa). It can be assumed that the change in geometry due to wear (and plastic deformation) has a negative influence on the wheel-rail interaction during the crossing of the frog, resulting in additional dynamic system forces due to vehicle excitations. The aim of this part of the project is to quantify the dynamic load input due to the respective geometry. As a first approach, the calculation method according to Jenkins is used. The basic principles of which are shown in Figure 25.

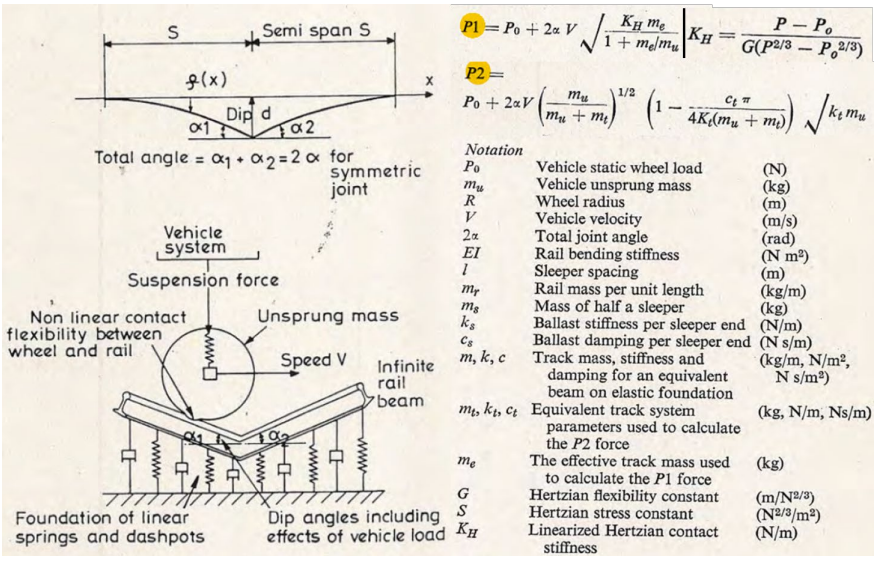

Figure 25 - P1/P2 calculation according to Jenkins [6]

The basic idea behind the calculation is that the failure characteristic happens with the help of the angle between the horizontal and the described wheel movement (see figure). This angle is basically a combination of the fault amplitude and the wavelength of the fault. Steep angles can be accompanied by a deep amplitude of the fault or by a short wavelength of the fault. This logic is consistent with the fact that short wavelengths result in higher dynamic loads than long wavelengths of the same amplitude, but the amplitudes of long wavelength faults are higher than for short wavelength faults. Further parameters are specific masses and stiffnesses of vehicle and track. These are necessary for an exact calculation of the dynamic forces, for a representation of the force development (x % higher dynamic load than with a new frog) realistic average values could be sufficient here. Another major influence is the vehicle speed. Figure 26 shows the typical time course of P1/P2 forces.

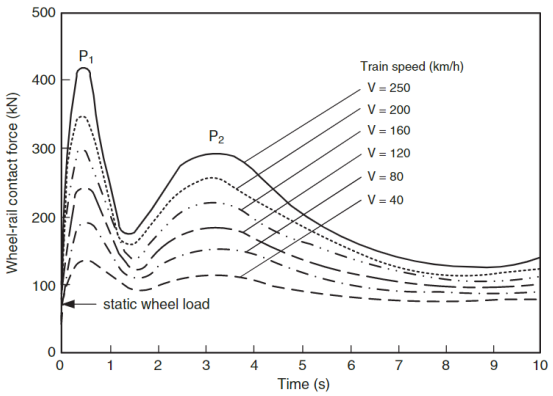

Figure 26 - Impact forces from a typical dipped joint [7]

The P1 force typically occurs directly due to the effect of the track. The amplitude of the P1 force is relatively large, the frequency is in a range which, according to the literature, is not very relevant for the ballast, as the forces are absorbed in the area of the rail/rail pad layers. However, the P1 force is certainly relevant for the damage of the rail or of the frog itself. The P2 (and subsequently P3, P4, ...) has a time-delaying effect and is triggered by the unsprung masses of the vehicle. The amplitude is usually smaller compared to the P1 force, but the frequency range is such that the P2 force causes damage to the ballast. As the ballast is the most critical element of track, in many cases only the P2 force is included in the evaluations. For the considerations of the frog, both P1 and P2 seem to be relevant. It can be seen from both the formal and Figure 26 that, according to this approach, the speed enters linearly into the force development.

Although originally developed for the evaluation of bolted rail joints, the original publication also includes considerations that this method can also be used for the evaluation of other effects (such as frogs). According to Jenkins, there are three points to consider here [6]:

1. The irregularity at a crossing occurs in one rail only. As the input, however, is asymmetric, the wheelset roll inertia will contribute to the effective vehicle unsprung mass.
2. Track mass and stiffness (particularly the former with cast manganese crossing noses) may at crossings be significantly different from the values for dipped joints.
3. The wavelength (or span) of a crossing irregularity is probably shorter than that at a dipped joint. The crossing geometry may also cause the effective angle at which the wheel strikes the crossing nose (the equivalent of 2α at a dipped joint) to vary with speed.

In the future, these uncertainties will be considered in the project, but at this point it should be discussed in principle how the approach can be transferred to the existing data situation. With the help of the Calipri measurements, the wheel trajectory during the crossing of the frog can be represented (considering a standard wheel profile). This was carried out by voestalpine, results in the curves shown in Figure 27.

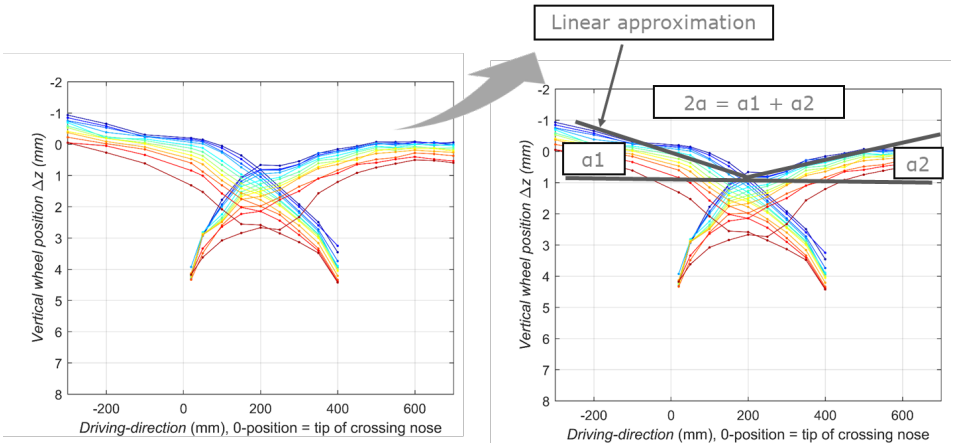

Figure 27 - Wheel trajectory - by geometry measurements

The blue wheel trajectory describes the wheel crossing according to the newly installed frog (2012), the red trajectory the wheel crossing according to the last existing measurement (2021). The descending curves represent the transition over the wing rail (if the frog was not present) and the descending curves the corresponding transition of the frog. At the intersection of two curves of the same colour, the wheel passes from the wing rail to the frog. It can be seen that the transition, due to wear and other effects, changes over the years. The position of the point of intersection decreases steadily and the angle of transition becomes steeper accordingly. It can be assumed that the dynamic loads increase consequently. In the last measurement (shown in dark red), there are already significant changes in the geometry and a retracted depression can be seen. This is probably the reaction to the high dynamic loads.

These data can easily be transferred into the Jenkins model. For this purpose, a linearization of the curves (right side of the figure) is carried out, according to which the angle necessary for the calculation can be taken. Consideration must be given to the number of measurement cross-sections taken into account, as this choice influences the calculated angle. Figure 28 shows this relationship.

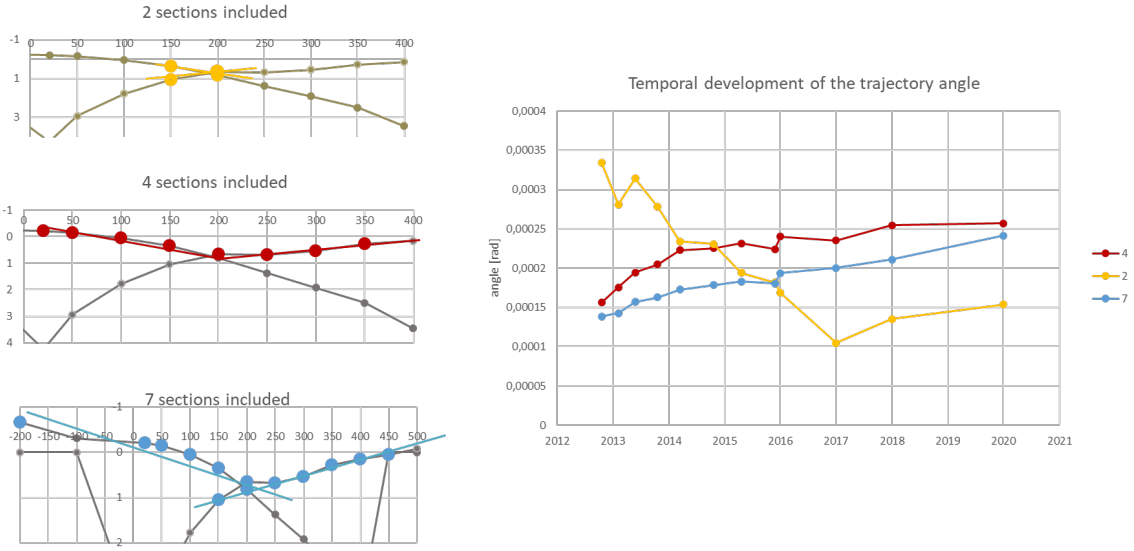

Figure 28 - Linearization process

Here, all of the existing measurements were linearized, considering three different scenarios. Scenario 1 (yellow) includes the two measurement cross-sections closest to the transfer position, scenario 2 (red) takes into account four cross-sections of the frog and the wing rail, scenario 3 (blue) seven measurements each. If we look at the change in angle over time, we see that Scenario 2 and Scenario 3 have similar curves, with the angle becoming steadily steeper, as expected. Scenario 1, however, shows a completely different behaviour and is therefore excluded for the time being. The question of which of the other scenarios better describes reality cannot yet be answered. It should be noted here that, all other parameters being equal, the measured angle enters linearly into the calculation of the dynamic forces. A difference in the angle of about 20% (as notable here between scenarios 2 and 3), therefore also leads to dynamic forces that differ by 20%. For this reason, additional attention will be paid to this issue.

In addition to the calculation of P1 and P2 forces according to Jenkins, other promising approaches can be found in the literature on how dynamic forces can be calculated analytically with the help of geometric input data (in particular the rail surface). The approach described in [8] should be highlighted here. In this approach, the first derivative of the geometry data is computed and, based on this, the maximum dynamic force is calculated. Although at first impression a different procedure is suspected, a similarity to Jenkins can be recognised. The first derivative of the vertical geometry measurement corresponds to the slope of this, which in turn correlates with the angle alpha shown in Jenkins. Details of the method, unless it is excluded for currently unknown reasons, will follow in future reports.

If one of the methods described here is successful, consideration can be given to using measurement data from a measurement vehicle for the evaluations. In the case of the EM250, only data from the LIDAR scanner are thinkable (for the frog), but it is unlikely that the resolution of the system is sufficient. However, there are already corresponding solutions on switch measuring wagons built for this purpose. Figure 29 shows an example of this.

Figure 29 - Turnout measurement car with geometrical measurements [9]

2.2.7 Outlook – Holistic evaluation

Due to its complexity, it is hardly possible to describe the condition of a frog on the basis of a single quality index. The six quality indicators presented here provide the opportunity to highlight one aspect at a time. Although correlations between the indicators are to be expected, blind spots cannot be ruled out when looking at only one index. A comprehensive description of the condition and prediction about future quality behaviour will only be possible through an intersection of the indicators. In the ongoing project, the focus will therefore lay on two things: 1) The further development of the presented quality indicators and 2) Exploring an increased understanding resulting from a meaningful intersection of several of the indicators.

2.3 Insulated rail joints as a critical part within turnouts

Insulated rail joints are the structural design of an electrical separation of two track sections. As turnouts, due to their function, always imply the delimitation of blocks, insulated rail joints in the turnout area or in the vicinity of turnouts are the rule. They are not by definition a component of turnouts; however, they must be considered for the condition assessment of turnouts. As being an inhomogeneity of the track, they can significantly influence the wheel-rail interaction. Experience over the last few years has shown that dynamic load input due to insulated rail joints can lead to ballast destruction at least on a level with the frog area. As the ballast is the critical element of the turnout, especially for turnouts with concrete sleepers, this circumstance can lead to significant costs. The poor track geometry resulting from the poor ballast condition causes additional dynamic forces within the system, which means that the tamping interval must be reduced. Ultimately, a point will be reached where the only choice left is between at least local ballast bed cleaning or renewal of the entire turnout.

In order to reduce the negative monetary influence of insulated rail joints in the turnout area, it could be an option to maintain or replace worn insulated rail joints before significant negative effects occur in the ballast. For this, however, it must be possible to describe the condition of insulated rail joints respectively the influence of the condition on the wheel-rail interaction (dynamic forces). As can be shown in 2.2.2 Report of Requirements, after the appropriate positioning of the measurement data, it is possible to evaluate the surface geometry of insulated rail joints by means of a rail surface signal. Figure 30 shows the typical signal characteristic of the RSS signal due to insulated rail joints.

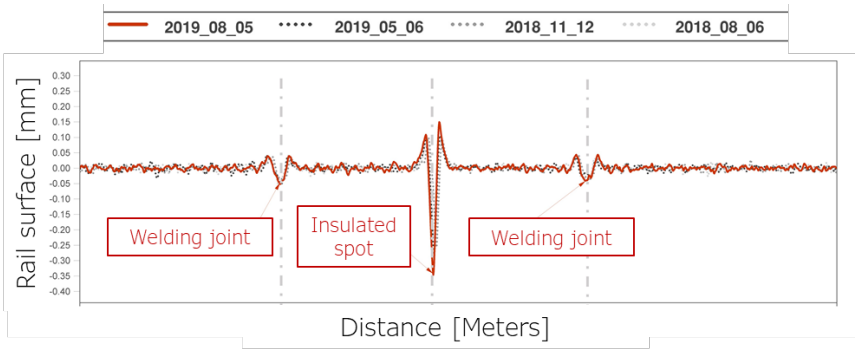

Figure 30 - Signal characteristic of insulated rail joints

As insulated rail joints (at least in Austria) are typically prefabricated and then welded into the track, this results in a typical characteristic with three deflections in the RSS signal. The two outermost deflections reflect the geometry of the two welding joints. These can have a significant influence on the wheel-rail interaction, but in most cases, they are not

dominant compared to the insulated spot. The middle deflection reflects the insulated spot itself. Since these are chord values of the RSS signal, a deconvolution of the signal must be implemented for an exact evaluation of the wheel-rail interaction or for simulations, but for an evaluation of the quality of the insulated rail joint and an approximation of the influence on the system interactions, it is expected that the consideration of the amplitudes of the raw signal could be sufficient. Further research is going on for this topic. The definition of a quality parameter can be done in different ways. 3 possibilities (Figure 31) were considered in relation to the condition description of insulated rail joints.

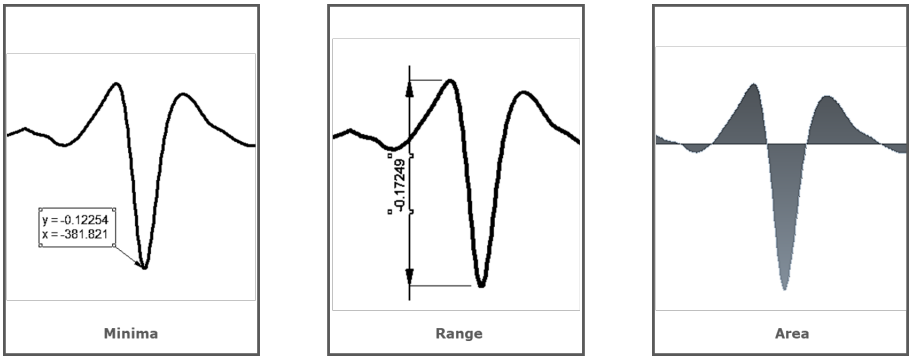

Figure 31 - Possible quality criteria

The first method describes characteristic values according to maximum values (in this case minimum values), the second method describes the distance between minimum value and maximum value and the third method characterises the effect by means of the enclosed area. We have excluded the latter method because the choice of the failure width has a significant influence on the index and the beginning and end of the defect cannot always be clearly defined, especially in the case of automation at a later stage. Evaluations show that a quality index according to peak-to-peak values and minimum values correlate very well with each other. For this reason, the simpler approach of the minimum value as a quality index is chosen. Figure 32 shows the development over time of the maximum amplitudes of the insulated rail joint.

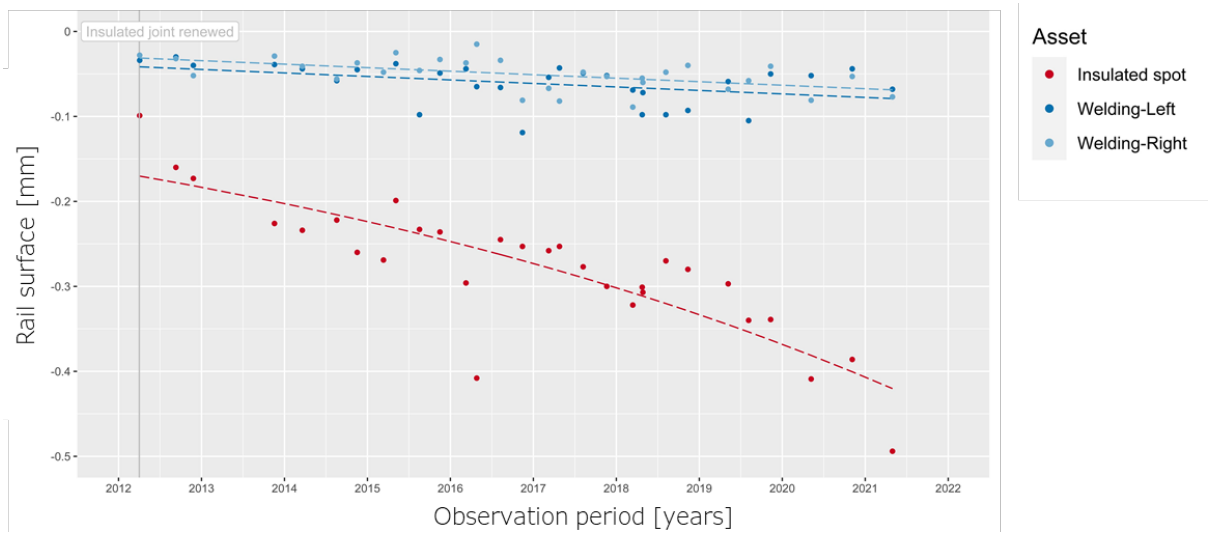

Figure 32 - Time series of the quality behaviour of insulated rail joints

The trend lines in blue describe the two welding joints, the red trend line the insulation spot. It can be seen that the welding joints have both a better initial quality (2012) than the insulating joint and experience less deterioration over time. The deterioration is to be considered linear for the welding joints and is associated with comparatively low rates. The insulating joint, on the other hand, appears to deteriorate in a superlinear manner with significantly higher deterioration rates. Current results indicate that already at amplitudes of the RSS signal as low as 0.15 mm, there is a significant influence on the development of single failures of the track geometry. If this is the case, the isolation spot shown here has already had a negative effect on the quality behaviour of the turnout since mid-2012. This circumstance is actually visible in the longitudinal level channel, as shown in Figure 33.

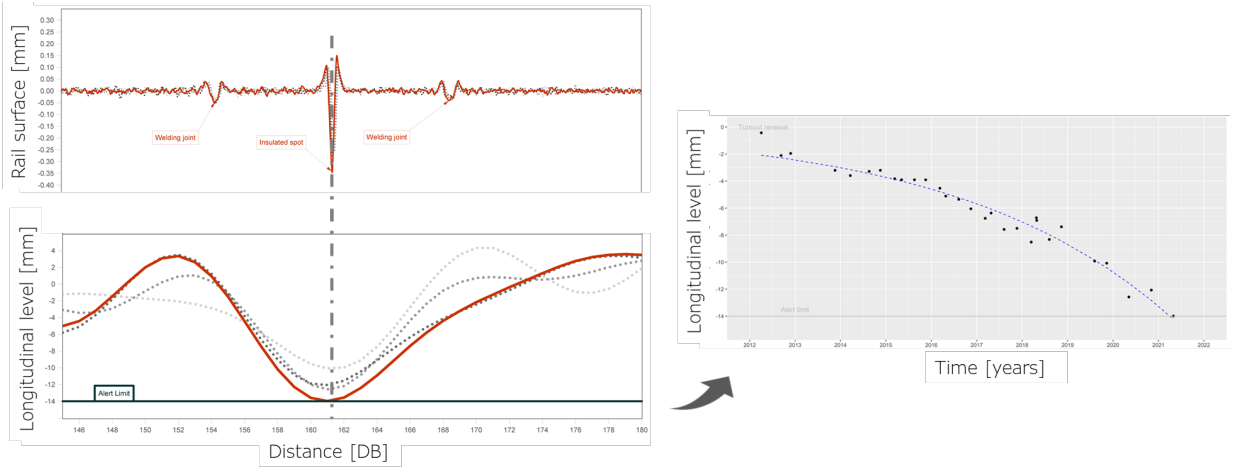

Figure 33 - Track geometry at the position of the insulated rail joint

Exactly at the position of the insulation spot, an isolated defect of the track geometry has developed, which reached the attention threshold in 2021. However, as can be seen on the right side of the figure, the growth has already started around 2012 and has consequently adopted a over-linear behaviour. Which part of the over-linear deterioration is due to the deteriorating quality of the insulated rail joint (short-wave wheel excitation) and which part can be attributed to the dynamic excitation due to the single failure of track geometry itself (medium-wave wheel excitation) cannot be answered at this point. The behaviour observed here could also be observed with other insulated rail joints, but not with all of them. The extent to which wear of insulated rail joints is systematic and how many insulated rail joints cause the described self-enhancing loop (statistical evaluation of the issue) is not part of this project, but are dealt with in the FFG-project NONIs – Neuentwicklung optimierter und nachhaltiger Isolierstoßsysteme. However, since insulated rail joints can have a significant influence on the quality behaviour of a turnout, they cannot be completely disregarded in the condition assessment of turnouts and are therefore considered in the description of system interrelationships within this project.

References

[1] M. Fellinger, Sustainable Asset Management for Turnouts - From measurement data analysis to behaviour and maintenance prediction, Graz: Verlag der Technischen Universität Graz, 2020.

[2] M. Sysyn, U. Gerber, O. Nabochenko, D. Gruen und F. Kluge, „Prediction of Rail Contact Fatigue on Crossings Using Image Processing and Machine Learning Methods," *Urban Rail Transit,* p. 123–132, 2019.

[3] Z. Fathollahi, A. Golroo und M. Bagheri, „Railway Turnout Defect Detection Using Image Processing," *International Journal of Transportation Engineering,* pp. 855-864, 2022.

[4] A. Haigermoser, B. Luber, J. Rauh und G. Gräfe, „Road and track irregularities: Measurement, assessment and simulation," *Vehicle System Dynamics,* pp. 878-957, 2015.

[5] U. Oßberger, W. Kollment und S. Eck, „Insights towards Condition Monitroing of Fixed Railway Crossings," *Procedia Structural Integrity,* pp. 106-114, 2017.

[6] H. H. Jenkins, J. E. Stephenson, G. A. Clayton, G. W. Morland und D. Lyon, „The Effekt of Track Vehicle PArameters on Wheel/Rail Vertical Dynamic Forces," *Railway Eng. J.,* pp. 2-16, 1974.

[7] A. M. Remennikov und S. Kaewunruen, „A review of loading conditions for railway track structures dueto train and track vertical interaction," *Structural Control and Health Monitoring,* Bd. 15, Nr. 2, pp. 207-234, 2008.

[8] . M. J. Steenbergen und C. Esveld, „Rail weld geometry and assessment concepts," *Proceedings of the Institution of Mechanical Engineers, Part F: Journal of Rail and Rapid Transit,* pp. 257-271, 2006.

[9] „Goldschmidt - Smat Rail Solutions," [Online]. Available: http://www.graw.com/en/track-measurement/turnout-measurement-system-tms.html. [Zugriff am 29 09 2022].

Institut für Eisenbahnwesen
und Verkehrswirtschaft
Technische Universität Graz
Rechbauerstrasse 12/II
8010 Graz
+43 316 873 6216
office.ebw@tugraz.at
www.ebw.tugraz.at